WADC TECHNICAL REPORT NO. 52-67

EXTRA COPY

MECHANICAL-PROPERTY TESTS ON CERAMIC BODIES

W. H. DUCKWORTH, A. D. SCHWOPE, O. K. SALMASSY,
R. L. CARLSON, and H. Z. SCHOFIELD

22 MARCH 1952

BATTELLE MEMORIAL INSTITUTE

20011221127

SECOND ANNUAL REPORT

on

MECHANICAL-PROPERTY TESTS ON CERAMIC BODIES

to

Wright-Patterson Air Force Base
Ohio

22 March 1952

Attention: Materials Laboratory
Engineering Division
MCREXM-3

Contract No. AF 33(038)-8682
Expenditure Order No. R605-233SR3A

by

W. H. Duckworth, A. D. Schwope, O. K. Salmassy,
R. L. Carlson, and H. Z. Schofield

Report for the Period of
18 November 1950 to 22 March 1952

BATTELLE MEMORIAL INSTITUTE
505 King Avenue
Columbus 1, Ohio

FOREWORD

This report was prepared by Battelle Memorial Institute, Columbus, Ohio, on Contract No. AF 33(038)-8682. Work at Battelle Memorial Institute was initiated as a project of the Materials Laboratory, Research Division, and is being accomplished under Expenditure Order No. R605-233SR3A. The work is being administered by the Materials Laboratory, Research Division, Air Development Command, with Mr. L. D. Richardson as Project Engineer. This report is the Second Annual Report, covering the period 18 November 1950 to 22 March 1952.

Among those who cooperated in the study were W. H. Duckworth, A. D. Schwope, O. K. Salmassy, R. L. Carlson, and H. Z. Schofield of Battelle Memorial Institute.

ABSTRACT

A critical survey was made of the significant theories of strength, for guidance in developing relationships among the strength properties of ceramics. The mechanistic theories appeared to offer the greater possibilities, but no theory treated all controlling variables, and all theories lacked adequate experimental support. The need remains apparent for a unified theory and supporting experimental data.

The principal laboratory effort was on the size dependence of strength. Both plaster and a nickel-titanium carbide body decreased in apparent strength with increases in gage-section size in bend tests. In an extensive program of bend tests on plaster to record details, strength decreased with increases in either gage-section length or gage-section breadth in about the same manner. However, the apparent strength increased with increases in gage-section depth. The possibility of the true size effect's being masked by size-dependent testing variables was indicated. There was no trend apparent in the standard deviation of strength values with variations of gage-section length, breadth, or depth.

Further information was obtained on the effect of the type of test on mechanical properties. Of particular interest is the fact that, with sufficient refinement, the bend and torsion tests appear to yield practically the same strength values. The development and refinement of tests was continued in an effort to obtain the precise mechanical-property data needed in this program.

TABLE OF CONTENTS

LIST OF ILLUSTRATIONS

LIST OF TABLES

WADC TECHNICAL REPORT NO. 52-67

SECOND ANNUAL REPORT

on

MECHANICAL-PROPERTY TESTS ON CERAMIC BODIES

to

WRIGHT-PATTERSON AIR FORCE BASE
OHIO

ATTENTION: MATERIALS LABORATORY
ENGINEERING DIVISION
MCREXM-3

CONTRACT NO. AF 33(038)-8682
EXPENDITURE ORDER NO. R605-233SR3A

from

BATTELLE MEMORIAL INSTITUTE

by

W. H. Duckworth, A. D. Schwope, O. K. Salmassy,
R. L. Carlson, and H. Z. Schofield

22 March 1952

INTRODUCTION

There is an active interest at present in the applicability of ceramic
materials for aircraft construction materials, particularly for parts of gas
turbines and jet engines. Design and evaluation studies are required. The
proper and efficient execution of these studies requires knowledge of the
mechanical behavior of ceramic bodies. Previous uses for these materials
have created little need for such knowledge, and little pertinent information
exists. The objective of this report is to augment this information.

An ultimate aim of the current work is to define strength properties
by expressions that include the influence of each external factor, thus per-
mitting design or evaluation studies with the fewest possible test data.

External factors to be considered include:

1. Stress system
2. Size
3. Rate of stressing
4. Temperature
5. Porosity

It is conceivable that this work could also establish the basic mechanisms of fracture; therefore, it might guide ceramic research in the development of bodies with improved internal structures. Research on flow and fatigue behavior is to be included when the studies of fracture are sufficiently advanced.

The above objectives require careful control of all possible variables through proper tests and testing techniques. It follows that much of the work must be devoted to analyses and development of means for accurately measuring stresses and strains. The types of test in the program are:

1. Tension
2. Compression
3. Torsion
4. Bend
5. Combined stress

Of primary concern in selecting materials for specimens is reproducibility, fabricability, and mechanical representation of one of the general types of ceramic bodies. Potential utility in aircraft also is of interest, but becomes secondary, in this fundamental study, to problems in determining the effects of external variables.

This is a rather long-range effort. The work was started in October, 1948, on a subcontract under Contract No. W33-038 ac 14105 between the Air Force and the RAND Corporation. It was taken over as a direct Air Force sponsorship during November, 1949.

The work for RAND is covered in RAND Report R-209, "Mechanical Properties of Ceramic Bodies", 31 August 1950. The bulk of this work was with porous and nonporous specimens of a silicate porcelain. Sintered-alumina specimens were used in a few investigations. Room-temperature, compression, torsion, and bend tests were made. The materials were elastic to fracture and exhibited isotropic behavior. Good correlation was obtained between elastic properties from the various tests, and an expression relating porosity and elastic moduli was developed. Observed strength phenomena could be explained qualitatively to some extent on the basis of a flaw-type mechanism of fracture.

Research during the first year of the direct Air Force sponsorship, from November, 1949, to November, 1950, is covered by AF Technical

Report No. 6512, April, 1951. This work was limited to K151A, a nickel-titanium carbide product of Kennametal, Inc. In room-temperature tension, compression, torsion, and bend tests, the material exhibited slight plastic flow. Relationships between elastic properties indicated isotropy. The mode of fracture in K151A was that normally found in brittle materials. Different fracture strengths were observed for the different types of test - tension, compression, torsion, and bending. During the course of testing, it became increasingly apparent that material variables in K151A were too great for proper execution of the research. A better controlled material would have to be selected. In view of this difficulty, any attempted quantitative correlation of strength values from the different tests was of questionable worth. Also, the problem was complicated by the observed plastic flow and by the presence of some bending in the tension, compression, and torsion tests. However, for the general case of brittle fracture, the data indicated again that a flaw-type mechanism offered the most likely basis for developing correlations. Elements involved include the theoretical strength, magnitude of the stress peaks, and a statistical function defining the number of peaks. A study of these elements was suggested.

The development and refinement of equipment and techniques has been carried on continuously in this research. During the period covered by AF Technical Report No. 6512, particular attention was given to high-temperature strain measurements.

The present report covers progress during the second year of direct Air Force sponsorship. The period covered is from 18 November 1950 to 22 March 1952. Work was recessed during three months of this period, however, for contractural processing.

During the period of this report, particular attention was given to the effect of size on fracture strength, using bend tests on plaster. Such work was considered essential to evaluating and developing theories from a flaw-type mechanism of fracture. As an important concurrent effort, a critical survey was undertaken of significant theories on strength.

REVIEW OF THEORIES OF STRENGTH

Historically, the strength properties of solids have been studied along two different lines. The oldest, the phenomenological, attempts to describe the reaction of a solid to an external stress system. Criteria of failure are postulated with the assumption that the solid is isotropic, homogeneous, and a continuum. By various methods of combining stresses, the effects of multiaxial stresses can be predicted. However, no single theory has been found to be applicable to all materials. This is not surprising in view of the many different types of mechanical behavior to be found. For example, some materials exhibit considerable flow before fracture, while others

fracture without any visible evidence of flow. The phenomenological approach, however, is important and useful in that, for any one material, a set of relations may be established which allows design calculations to be made. Thus, the material can be used to its fullest advantage.

The second approach is mechanistic in nature. Here, the strength properties are analyzed from the point of view of what makes the material fail. These theories are relatively new, and are concerned with the fact that materials may fracture at stresses 100 to 1000 times below their theoretical breaking strength. The presence of defects such as cracks, dislocations, and other possible flaws is postulated, and the behavior of a material containing such flaws is predicted. Although this approach appears to be the more fundamental of the two, a thorough understanding of the phenomenological theories is necessary for intelligent use of the mechanistic theories.

Phenomenological Theories

Each of the phenomenological theories is based upon some assumed criterion for failure. In general, these theories place no restrictions on the nature of the material to which they are to be applied. They have been used to predict failure in both brittle and ductile materials.

All of the phenomenological theories assume homogeneity and isotropy of the material, and the criteria which these theories set up are based on relations of stress and strain evolved from the classic theory of elasticity. These relations are of particular significance in the analysis of combined stresses.

As a guide to the phenomenological approach, it is well to review the methods of analysis applicable to combined stresses. Since the biaxial stress condition is found more commonly than triaxial stresses in service, the development of the theories will be limited as much as possible to the biaxial case.

In the general case of two-dimensional or biaxial stress, the free-body diagram shown in Figure 1 is appropriate. The forces acting on the tz plane are unknown, but vary as the angle θ varies. There is one position for which the normal force F_n is a maximum. To find this, the relationship between F_n and θ must be determined first. This is done by considering the summation of forces in the n direction, as follows:

$$F_n = F_x \sin\theta + F_{yx} \cos\theta + F_y \cos\theta + F_{xy} \sin\theta. \qquad (1)$$

To convert the forces to stress components, it is necessary to divide by the area over which the forces act. Equation (1) can be rewritten in terms of stresses, assuming $\tau_{xy} = \tau_{yx}$[*]:

---

[*] The symbol σ denotes a normal stress; the symbol τ denotes a shear stress.
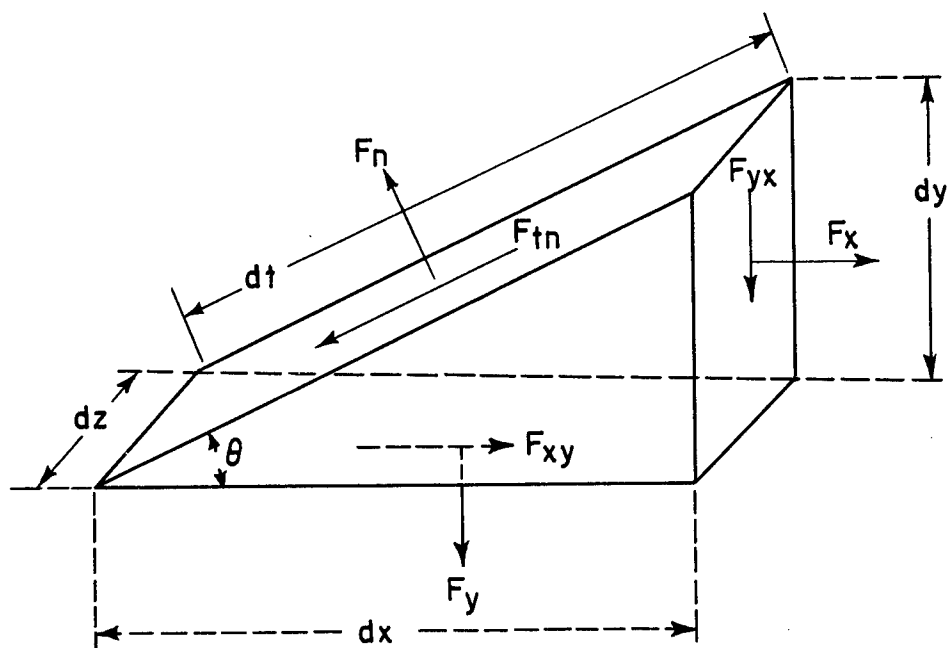
FIGURE I. GENERAL BIAXIAL-FORCE DIAGRAM
A-2185

$$\sigma_n = \sigma_x \sin^2 \theta + \sigma_y \cos^2 \theta + \tau_{xy} \sin 2\theta. \tag{2}$$

To determine the angle θ for which σ_n becomes a maximum or minimum, it is necessary only to differentiate Equation (2) with respect to θ; thus:

$$\frac{d \sigma_n}{d\theta} = 2 \sigma_x \sin\theta \cos\theta - 2 \sigma_y \sin\theta \cos\theta + 2 \tau_{xy} \cos 2\theta = 0.$$

Then, using $2 \sin\theta \cos\theta = \sin 2\theta$, the direction for the maximum or minimum normal stress is given by:

$$\tan 2\theta = \frac{-2 \tau_{xy}}{\sigma_x - \sigma_y}. \tag{3}$$

In order to calculate the magnitude of the normal stress from Equation (2), $\sin 2\theta$ and $\cos 2\theta$ must be determined. From examination of Equation (3), these are:

$$\sin 2\theta = \frac{-2 \tau_{xy}}{\pm \left[(\sigma_x - \sigma_y)^2 + 4 \tau_{xy}^2 \right]^{1/2}}, \tag{4}$$

and

$$\cos 2\theta = \frac{(\sigma_x - \sigma_y)}{\pm \left[(\sigma_x - \sigma_y)^2 + 4 \tau_{xy}^2 \right]^{1/2}}. \tag{5}$$

Using $\sin^2\theta = \left(\dfrac{1 - \cos 2\theta}{2}\right)$ and $\cos^2\theta = \left(\dfrac{1 + \cos 2\theta}{2}\right)$ and substituting into Equation (3), the expression for the maximum and minimum normal stresses becomes:

$$\sigma_n = \frac{\sigma_x + \sigma_y}{2} \pm \left[\left(\frac{\sigma_x - \sigma_y}{2}\right)^2 + \tau_{xy}^2\right]^{1/2}. \tag{6}$$

The stresses $\sigma_{n(max)}$ and $\sigma_{n(min)}$ commonly are called principal stresses and will be designated as σ_1 and σ_3. The reason for not using σ_2 as the minimum normal stress will become evident later, where intermediate stresses will be used and designated as σ_2.

The values of the maximum and minimum shearing stresses (τ_s) can be derived similarily and the final expression is:

$$\tau_s = \pm \left[\left(\frac{\sigma_x - \sigma_y}{2}\right)^2 + \tau_{xy}^2\right]^{1/2}. \tag{7}$$

The criteria of maximum normal and shearing stresses have been used extensively in the development of theories describing a material's reaction to multiaxial stress systems. All of the theories have been developed on the basis of the free-body diagram in Figure 1, and the development of Equations (1) through (7) will be referred to frequently in the following discussion of these theories.

Maximum-Stress Theory

The maximum-stress theory assumes, in the case of brittle materials, that fracture starts in an element subjected to combined stresses when the maximum principal stress becomes equal to the fracture stress of the material in tension. Stated analytically for the three-dimensional case:

$$\sigma_f = \pm \sigma_1, \tag{8}$$

where σ_f = fracture strength in simple tension, and where the principal stresses σ_1, σ_2, and σ_3 are such that:

$$\sigma_2 < \sigma_1 > \sigma_3.$$

In this form, the theory assumes equal strengths in compression and tension. Often it is convenient to designate the compression stress as σ_3 and then the breaking strength (σ_f) in compression becomes:

$$-\sigma_f = \sigma_3, \tag{9}$$

where $\sigma_2 < \sigma_3 > \sigma_1$.

Expressed in terms of the stress components, the fracture stress is given as:

$$\sigma_f = \frac{\sigma_x + \sigma_y}{2} \pm \left[\left(\frac{\sigma_x - \sigma_y}{2} \right)^2 + \tau_{xy}^2 \right]^{1/2} , \tag{10}$$

which is identical to Equation (6) for the maximum normal stress.

A modified form of this theory assumes that, if one of the three principal stresses is positive (tension), the limiting value is less than if all the stresses are negative (compression). Although this is closer to the truth for materials exhibiting brittle behavior, it is extremely artifical and cannot be considered an important relationship.

The maximum-stress theory is used commonly in design when materials exhibiting brittle behavior are used. Two of the more common criteria for brittle behavior are that the fracture surface is normal to the specimen axis in a tension test and at an angle of 45° in a torsion test. Such behavior will be assumed for materials classed as brittle in this report.

Maximum-Strain Theory

This theory assumes that failure occurs when the positive elastic strain in the direction of one of the principal stresses becomes equal to the value at failure in tension. The principal elastic strains are given by the relationships:

$$\epsilon_1 = \pm \frac{1}{E} \left[\sigma_1 - \nu (\sigma_2 + \sigma_3) \right] ,$$

$$\epsilon_2 = \pm \frac{1}{E} \left[\sigma_2 - \nu (\sigma_1 + \sigma_3) \right] , \tag{11}$$

and

$$\epsilon_3 = \pm \frac{1}{E} \left[\sigma_3 - \nu (\sigma_1 + \sigma_2) \right] ,$$

where ν = Poisson's ratio,

   E = Young's modulus.

If, then, the limiting strain in tension is given as ϵ, failure will occur when ϵ_1, ϵ_2, or ϵ_3 become equal to ϵ. This can be stated in terms of stresses. If $\sigma_f = \epsilon_E$, then

$$\sigma_f = \sigma_1 - \nu (\sigma_2 + \sigma_3) . \tag{12}$$

In terms of stress components and considering only planar stress, Equation (12) becomes:

$$\sigma_f = (1 - \nu)\left(\frac{\sigma_x + \sigma_y}{2}\right) + (1 + \nu)\left[\left(\frac{\sigma_x - \sigma_y}{2}\right)^2 + \sigma_{xy}^2\right]^{1/2} \quad (13)$$

If the stress system is uniaxial compression, the lateral strains are positive and equal to $\nu\, \sigma_c/E$. Then the material is expected to fail when the lateral strain equals the longitudinal strain at failure in a tension test. The compression stress at failure is then σ_f/ν, which is 3 to 8 times the tension-failure stress, depending on Poisson's ratio. It can be seen that, if a hydrostatic pressure were superposed on the compression stress, the material could not fracture and brittle materials could be made to flow. Such an effect was found by Bridgman[1] in tests on the brittle materials, glass, Carboloy, and alumina.

Maximum-Shear-Stress Theory

This theory assumes that failure of materials occurs when the shear stress reaches a maximum. It should be stated that this theory has been used widely when failure is defined as a yielding, rather than fracturing. Thus, its applicability to materials exhibiting no flow is not immediately apparent. The theory was used first because it was noticed that yielding occurred on planes making an angle of 45° with the principal stress direction. In terms of principal stresses, the maximum shear stress is given by:

$$\tau_m = \frac{\sigma_1 - \sigma_3}{2} \quad . \quad (14)$$

For the limiting case of tension or compression,

$$\tau_m = \frac{\sigma_1}{2} = -\frac{\sigma_3}{2} \quad ;$$

therefore: $$\sigma_f = 2\,\tau_m = \sigma_1 - \sigma_3 \quad . \quad (15)$$

The presence of an intermediate stress in a triaxial stress system is not considered to affect the value of the critical shear stress. In terms of stress components, Equations (14) and (15) yield:

$$\sigma_f = 2\left[\left(\frac{\sigma_x - \sigma_y}{2}\right)^2 + \tau_{xy}^2\right]^{1/2} \quad , \quad (16)$$

which is identical in form to Equation (7).

It is noted that this theory, as well as the maximum-normal-stress theory, does not assume strain to be proportional to stress, as does the maximum-strain theory. However, it has the disadvantage that intermediate stresses are not considered operative. This may be the case for flow criteria, but it is well known that such stresses alter fracture strengths.

Maximum-Strain-Energy Theory

The quantity of strain energy stored per unit volume also has been used as a criterion for failure. Failure is expected, according to this law, when the strain energy stored as a result of combined stresses equals the strain energy at failure in tension. The total strain energy stored per unit volume in a multiaxial stress system is given as:

$$W = 1/2 \left(\sigma_1 \epsilon_1 + \sigma_2 \epsilon_2 + \sigma_3 \epsilon_3 \right) \quad . \tag{17}$$

This can be restated in terms of stresses by substituting Equation (11) for the strains, resulting in the expression:

$$W = 1/2E \left(\sigma_1^2 + \sigma_2^2 + \sigma_3^2 \right) - \nu/E \left(\sigma_1 \sigma_2 + \sigma_2 \sigma_3 + \sigma_3 \sigma_1 \right). \tag{18}$$

The strain energy at fracture in tension is given by:

$$W_f = \frac{\sigma_f^2}{2E} \quad . \tag{19}$$

By combining Equations (18) and (19), the expression for the fracture stress becomes:

$$\sigma_f = \left[\sigma_1^2 + \sigma_2^2 + \sigma_3^2 - 2\nu \left(\sigma_1 \sigma_2 + \sigma_2 \sigma_3 + \sigma_3 \sigma_1 \right) \right]^{1/2} , \tag{20}$$

or, expressed in terms of stress components:

$$\sigma_f = \left[\sigma_x^2 + \sigma_y^2 + \sigma_z^2 - 2\nu \left(\sigma_x \sigma_y + \sigma_y \sigma_z + \sigma_z \sigma_x \right) \right.$$
$$\left. + 2 \left(1 + \nu \right) \left(\tau_{xy}^2 + \tau_{yz}^2 + \tau_{zx}^2 \right) \right]^{1/2} \quad . \tag{21}$$

This theory assumes strain to be proportional to stress, and the tension and compression strengths to be equal. This theory has been superseded largely by the distortion-energy theory, so little will be said of it here. Also, the maximum-strain-energy theory has been applied to the plastic flow of solids.

Distortion-Energy Theory

This theory assumes that failure begins when the energy of shear of any stress system reaches the energy at failure in simple tension. It has been extremely successful in describing the flow of ductile materials, and is felt to have potential utility in the field of brittle behavior. The distortion-energy theory assumes strain to be proportional to stress and considers that the total energy stored in a material is composed of two parts, distortion and dilatation. The expression for dilatation is given by:

$$\sigma_v = \frac{\sigma_1 + \sigma_2 + \sigma_3}{3} \quad , \tag{22}$$

which is referred to often as the hydrostatic stress. The strain energy due to the dilatation then is given as:

$$U_v = 3 \; \frac{\sigma_v \epsilon_v}{2} = \frac{3}{2} \; \epsilon_v \left(\sigma_1 + \sigma_2 + \sigma_3\right) \quad . \tag{23}$$

Also, since:

$$\epsilon_v = \left(\frac{1 - 2\nu}{E}\right) \sigma_v \quad , \tag{24}$$

then:

$$U_v = \frac{1 - 2\nu}{6E} \left(\sigma_1 + \sigma_2 + \sigma_3\right) \quad . \tag{25}$$

To obtain the distortion energy (V), Equation (25) is subtracted from the total strain energy, as given by Equation (18), with the result:

$$V = \frac{1 + \nu}{6E} \left[\left(\sigma_1 - \sigma_2\right)^2 + \left(\sigma_2 - \sigma_3\right)^2 + \left(\sigma_3 - \sigma_1\right)^2\right] \quad . \tag{26}$$

The distortion energy at failure in tension ($\sigma_1 = \sigma_f$) is given then as:

$$V = \left(\frac{1 + \nu}{3E}\right) \sigma_f^2 \quad . \tag{27}$$

Therefore, failure occurs when the energy in a combined stress system equals that in uniaxial tension at failure. The distortion-energy relation becomes:

$$\sigma_f = \frac{1}{\sqrt{2}} \left[(\sigma_1 - \sigma_2)^2 + (\sigma_2 - \sigma_3)^2 + (\sigma_3 - \sigma_1)^2 \right]^{1/2},$$

(28)

$$\sigma_f = \left[\sigma_1^2 + \sigma_2^2 + \sigma_3^2 - (\sigma_1 \sigma_2 + \sigma_2 \sigma_3 + \sigma_3 \sigma_1) \right]^{1/2},$$

or, in terms of stress components:

(29)

$$\sigma_f = \frac{1}{\sqrt{2}} \left[(\sigma_x - \sigma_y)^2 + (\sigma_y - \sigma_z)^2 + (\sigma_z - \sigma_x)^2 + 6(\tau_{xy}^2 + \tau_{yz}^2 + \tau_{zx}^2) \right]^{1/2}.$$

If the stress system is two dimensional, Equation (29) reduces to:

$$\sigma_f = (\sigma_x^2 + \sigma_y^2 - \sigma_x \sigma_y + 3\tau_{xy}^2)^{1/2}.$$

(30)

The distortion-energy theory assumes equal strengths in compression and tension. As has been mentioned, it has been successful mainly in describing the yielding or flow of materials.

Internal-Friction Theory

This modification of the maximum-shear-stress theory was proposed to account for the fact that failure in tension did not occur on a 45° plane. It is formulated by assuming that there is a resistance to sliding on the plane of shear (dzdt in Figure 1) which is composed of the shearing stress plus a frictional component. The general statement of this theory is:

$$\tau_m = \frac{1}{2 \cos \alpha} \left[(\sigma_1 - \sigma_3) + (\sigma_1 + \sigma_3) \sin \alpha \right],$$

(31)

where $\alpha = \tan^{-1} f$,

f = coefficient of friction.

For simple tension:

$$\tau_m = \frac{\sigma_1 (1 + \sin \alpha)}{2 \cos \alpha},$$

(32)

and the failure under combined stresses relative to the tension-failure stress is given as:

$$\sigma_f = \sigma_1 - \sigma_3 \frac{(1 - \sin a)}{(1 + \sin a)} \quad . \tag{33}$$

It is seen that, if $a = 0$, Equation (33) reduces to that of the maximum-shear-stress law [Equation (15)].

If $\sin a = 0.2$, the compression strength should be 1.5 times the tension strength, and the torsion strength should be 0.6 times the tension strength. Thus, by choosing the correct value of $\sin a$, the experimental evidence of the compression strength's being higher than the tension strength in brittle materials can be supported analytically.

Mohr Theory

Another variation in the maximum-shear theory was introduced by Mohr[2]. It assumes that some plane other than the plane dzdt in Figure 1 is the plane of maximum shear stress. Mohr's theory was developed graphically, and only the final equations will be stated in this brief review. The maximum principal shear stress is given by:

$$\tau_m = \left(\frac{\sigma_1 - \sigma_3}{2}\right) \sin 2\theta \quad , \tag{34}$$

and the maximum normal stress is given by:

$$\sigma_n = \left(\frac{\sigma_1 + \sigma_3}{2}\right) + \left(\frac{\sigma_3 + \sigma_1}{2}\right) \cos 2\theta \quad . \tag{35}$$

Since the maximum shearing stress is the criterion for failure, the failure stress is given as:

$$\tau_m = \frac{\sigma_1}{2} \quad , \tag{36}$$

and

$$\sigma_f = 2 \tau_m = \sigma_1 \quad ,$$

where $\theta = 45°$.

This theory also can be expressed in the more useful form given by Timoshenko[2] which relates the failure strengths in shear (τ_{fs}), tension (σ_{ft}), and compression (σ_{fc}):

$$\tau_{fs} = - \frac{\sigma_{ft} \, \sigma_{fc}}{\sigma_{ft} - \sigma_{fc}} \quad . \tag{37}$$

If $\sigma_{ft} = - \sigma_{fc}$, then $\tau_{fs} = 1/2\ \sigma_{ft}$. Since, in brittle materials, the strengths in compression and tension are different, Equation (36) enables adjustment for this fact. If the compression strength is 8 times the tension strength, the shear strength should be 0.89 of the tension strength.

Mohr's theory is very general and, because of its flexibility, has been modified by many investigators to fit their data. Therefore, it loses importance and becomes little more than an empirical observation, the form of which varies with the material.

A modification of Mohr's theory has been proposed by Marin[3] which recognizes the difference between compression and tension strengths. It can be stated analytically as:

$$(y/x)^2\ (x - y)^2\ (-4k - 4k^2) + (2y/x)\ (x^2 - y^2 + x - y) + (x + y)^2$$
$$+ 2\ (x + y) + (1 + 2k)^2\ (x - y)^2 - 4\ (k + k^2) = 0 \quad , \tag{38}$$

where $x = \sigma_1 / \sigma_c$,

$y = \sigma_2 / \sigma_c$,

σ_c = compressive strength,

k = constant.

The constant k can be evaluated if the ratio of the tension to the compression strength is known, and Equation (38) solved for the case of pure tension. The modification permits the effects of any multidimensional stress system to be evaluated without assuming the tension and compression strengths to be equal. However, it is semiempirical and is rather cumbersome to use for design work.

Stress-Invariant Theory

In connection with the work on this project, a relationship has been suggested by L. R. Jackson of the Battelle staff to account for the difference between the tension and compression strengths of ceramics. In a solid with normal stresses acting on the three mutually perpendicular faces, the equilibrium of the stresses on any plane through the solid can be written as:

$$\sigma_x{}' = \sigma_x\ l + \tau_{yx}\ m + \tau_{zx}\ n,$$

$$\sigma_y{}' = \tau_{xy}\ l + \sigma_y\ m + \tau_{zy}\ n, \tag{39}$$

$$\sigma_z{}' = \tau_{xz}\ l + \tau_{yz}\ m + \sigma_z\ n,$$

where $\sigma_x{}'$, $\sigma_y{}'$, $\sigma_z{}'$ = components of the resultant stress σ' on any plane,

1, m, n = direction cosines of this plane.

Now, if this plane carries only a normal stress σ and no shearing stress, the components become:

$$\sigma_x{}' = \sigma \, 1 \ ,$$

$$\sigma_y{}' = \sigma \, m \ ,$$

$$\sigma_z{}' = \sigma \, n \ .$$

If a principal plane of stress is considered, Equation (39) can be expressed in determinant form as:

$$\begin{bmatrix} \sigma_x - \sigma & \tau_{yx} & \tau_{zx} \\ \tau_{xy} & \sigma_y - \sigma & \tau_{zy} \\ \tau_{xz} & \tau_{yz} & \sigma_z - \sigma \end{bmatrix} = 0 \qquad (40)$$

Evaluating this determinant, the term I_3 and the coefficients I_1 and I_2 of the σ^2 and σ terms are found to be:

$$I_1 = \sigma_x + \sigma_y + \sigma_z \ , \qquad (41)$$

$$I_2 = \sigma_x \sigma_y + \sigma_y \sigma_z + \sigma_z \sigma_x - (\tau_{xy}{}^2 + \tau_{yz}{}^2 + \tau_{zx}{}^2) \ , \qquad (42)$$

$$I_3 = \sigma_x \sigma_y \sigma_z + 2 \, \tau_{yz} \tau_{xz} \tau_{xy} - \sigma_x \tau_{yz}{}^2 - \sigma_y \tau_{xz}{}^2 - \sigma_z \tau_{xy}{}^2 \ , \qquad (43)$$

where I_1, I_2, and I_3 are commonly called the stress invariants. The hydrostatic stress is seen to be $I_1/3$ and, in the common usage of these invariants, is not considered to influence the plastic flow of materials. Using this principal, Nadai[4] has subtracted the hydrostatic component from Equation (42), and derived a criterion for the flow of solids known as the octahedral shearing stress. He assumed that the oblique plane cutting through the solid, which was used for the derivation of Equation (39), makes an angle of 54°45' with the principal axis. His relationship can be expressed then as:

$$\tau_{oct} = 1/3 \left[(\sigma_1 - \sigma_2)^2 + (\sigma_2 - \sigma_3)^2 + (\sigma_3 - \sigma_1)^2 \right]^{1/2} \ , \qquad (44)$$

or, in terms of stress components:

$$\tau_{oct} = 1/3 \left[(\sigma_x - \sigma_y)^2 + (\sigma_y - \sigma_z)^2 + (\sigma_z - \sigma_x)^2 \right.$$

$$\left. + 6 (\tau_{xy}^2 + \tau_{yz}^2 + \tau_{zx}^2) \right]^{1/2} \quad . \tag{45}$$

Although its form is rather different, the octahedral stress can be considered to be the equivalent of I_2 multiplied by a constant. Since this form has the hydrostatic component subtracted from it, and realizing that fracture of solids differs from flow in that fracture is dependent upon the hydrostatic pressure, it is reasonable to add the invariant I_1 to Equation (45). This could be accomplished by combining it directly in τ_{oct}; however, it was found that better agreement was obtained by adding I_1 to Equation (45), so that:

$$\sigma_f = 1/3 \left[(\sigma_x - \sigma_y)^2 + (\sigma_y - \sigma_z)^2 + (\sigma_z - \sigma_x)^2 \right.$$

$$\left. + 6 (\tau_{xy}^2 + \tau_{yz}^2 + \tau_{zx}^2) \right]^{1/2} + \frac{\sigma_x + \sigma_y + \sigma_z}{3} \quad . \tag{46}$$

Then, for tension:

$$\sigma_f = \frac{(2)^{1/2}}{3} \sigma_x + \frac{\sigma_x}{3} = 0.805 \, \sigma_x , \tag{47}$$

and, for torsion:

$$\sigma_f = \left(\frac{2}{3} \right)^{1/2} \tau_{xy} = 0.816 \, \tau_{xy} . \tag{48}$$

The relation between the torsion and tension strengths becomes:

$$\sigma_x = 1.015 \, \tau_{xy} . \tag{49}$$

The fracture criterion for compression (σ_x') is given as:

$$\sigma_f = - \frac{(2)^{1/2}}{3} \sigma_x + \frac{\sigma_x}{3} = -0.138 \, \sigma_x , \tag{50}$$

and the relationship between tension and compression strengths:

$$\sigma_x' = -5.84 \, \sigma_x . \tag{51}$$

The usual method of making compression tests in the laboratory results in a stress system which is not pure compression, as pointed out in AF Technical Report No. 6512. Assuming that no bending stresses are present, stresses still arise from the restraint of differential lateral strains by friction between the specimen and the loading faces. Considering these additional stresses, it follows that:

$$\sigma_x' = k \sigma_y' = k \sigma_z \ . \tag{52}$$

Substituting Equation (52) into Equation (50), the general expression for the compression strength is given as:

$$\sigma_f = \left[- \frac{(2)^{1/2}}{3} (1 - k) + \frac{1 + 2k}{3} \right] \sigma_x' \ . \tag{53}$$

The effect of these other stresses can be seen by letting k in Equation (52) equal 0.05; then the ratio between the compression and tension strengths increases to 12.7. It is possible, by adding a sufficient hydrostatic component, that the material will have an infinite fracture strength, and failure will occur by some other mechanism, such as plastic flow.

Equally valid relationships can be derived if, instead of the octahedral-stress theory, the effective-stress theory is used. The two differ only in the constant; in the octahedral theory it is 1/3, in the effective-stress theory it is $1/\sqrt{2}$. If the latter is used, the relations given by Equations (47) through (51) become:

for tension:

$$\sigma_f = \sigma_x + \frac{\sigma_x}{3} = 1.33 \sigma_x \ , \tag{54}$$

and for torsion:

$$\sigma_f = \sqrt{3} \ \tau_{xy} = 1.73 \ \tau_{xy} \ , \tag{55}$$

and the ratio between tension and torsion:

$$\sigma_x = 1.3 \ \tau_{xy} \ . \tag{56}$$

The criterion for fracture in compression then becomes:

$$\sigma_f = - \sigma_x + \frac{\sigma_x}{3} = -0.67 \sigma_x' \ , \tag{57}$$

and the ratio of compression to tension strengths:

$$\sigma_x' = 2 \sigma_x \ . \tag{58}$$

The equation analogous to Equation (53) is then:

$$\sigma_f = (-0.67 + 1.66 \text{ k}) \sigma_x' , \tag{59}$$

and, if k = 0.05, the ratio between the compression and tension strengths increases to 2.3. The rate of increase of strength with increasing values of k is much slower using Equation (59) than using Equation (53). Using Equation (53) and the ratio of strength in torsion and tension, it should be possible to evaluate the relative merits of the two sets of relationships.

General Comments on Phenomenological Theories

It is evident that there are a large number of theories purporting to describe relationships among the strength properties under various stress systems. To date, there is no single theory which will correlate the properties of all materials. For materials which exhibit plastic flow, the maximum-shear-stress, the distortion-energy, and the octahedral- or effective-stress theories provide the best fit. For materials which evidence little or no plastic flow before fracture (brittle behavior), the maximum-normal-stress and maximum-strain theories and variations of the Mohr theory have been successful. However, none of these predict the material to be stronger in compression than in tension. To satisfy this requirement, the stress-invariant theory has been proposed.

Many problems remain to be solved. Experimental work shows that the effect of size is quite significant in brittle materials. Brittle materials supposedly contain many microflaws. Therefore, the application of statistics to strength properties is necessary, and should be a valuable tool in understanding the size effect. However, statistics can be applied only when the basic relationships among strengths under various stress systems are known. The phenomenological approach to the strength problem is a logical starting point for such work.

Mechanistic Theories

The mechanistic theories attempt to explain fracture phenomena, rather than relate strength values, as do the phenomenological theories. All of these theories assume the presence in a material of discontinuities of such a nature as to cause stress concentrations whose effect is to reduce the apparent breaking strength to a value far below the theoretical strength. The magnitude of the stress concentrations resulting from the discontinuities is larger than can be predicted by the classic theory of elasticity, causing the obvious inference that the flaws are of submicroscopic size.

Although the mechanistic theories postulate a mechanism of fracture, they still require an assumption of the criterion for fracture, as do the phenomenological theories. Fracture still is considered to occur at some

condition of stress or strain. Nevertheless, the mechanistic theories have the advantage of providing a word picture of fracture phenomena.

Griffith Crack Theory

Griffith developed his theory in an attempt to explain the extraordinary weakening of materials by surface scratches whose areas were but a minute part of the cross-sectional area of the material. He assumed that the scratches or cracks acted as stress concentrators and that, at their extremities, the stress reached approximately the theoretical strength of the material. The calculations of Inglis[5] were used to determine the stresses and strains resulting from typical scratches. The predictions of these calculations were borne out by tests.

Griffith started from the "theorem of minimum energy". This theory states that an elastic body distorted by external forces reaches an equilibrium condition when the potential energy of the whole system has been minimized. To obtain his fracture theory, he added that the equilibrium position is one in which the body has fractured if, in fracturing, the system has passed from the stressed state to the fractured state by a continuous decrease in potential energy. The increase of potential energy which is occasioned by the new surface formed by the initiation or extension of a crack must not be neglected, however. In a stressed body, the elastic energy must provide this surface energy, which is 2α for a unit cross section, where α is the specific surface energy.

Theoretically, the fracture strength of a flawless brittle substance should be the value of its "intrinsic pressure", and can be calculated from:

$$S_m = \sqrt{\frac{2\,\alpha\,E}{a}} \quad , \tag{60}$$

where S_m = the molecular cohesion (theoretical strength),

   E = Young's modulus,

   a = the atomic spacing.

Griffith assumed that, in the regions of stress concentration around flaws, the theoretical strength of the material is reached in very small volumes of the specimen. From the Inglis calculations, Griffith, by assuming the crack to be a very flat elliptical hole of major axis 2c, found the maximum stress at the ends of the crack to be:

$$S_m = 2\,\sigma\sqrt{\frac{c}{r}} \quad , \tag{61}$$

where σ = the macroscopic stress perpendicular to the major axis of the crack,
   r = the radius of curvature at the ends of the major axis.

It is seen that the maximum stress will increase toward infinity as the radius of curvature r approaches zero; however, it becomes impossible to conceive a radius of curvature smaller than the interatomic spacing of the material. If the value of the interatomic spacing a is substituted for r in Equation (61), which is then divided by Equation (60), the result is the applied stress which will cause a microscopic stress equal to the theoretical strength at the ends of a crack with r = a. The relation then becomes:

$$\sigma = \sqrt{\frac{a E}{2c}} \quad . \tag{62}$$

As will be seen later, this value differs only slightly from the value given by Griffith [Equation (68)] and may be explained quite well by the inapplicability of Hooke's Law at the high stress values which are obtained.

Surface cracks of depth c produce approximately the same stress concentration as internal cracks of length 2c. From the stress distribution around an elliptical hole, the increase of elastic energy of a plate by the introduction of a crack is:

$$W_e = \frac{\pi c^2}{E} \sigma^2 \quad , \tag{63}$$

per unit thickness, if the plate is thin (thickness < 2c). If the case of plane strain holds (thickness > 2c), the increase is:

$$W_e = 1 - \nu^2 \frac{\pi c^2}{E} \sigma^2 \quad , \tag{64}$$

where ν = Poisson's ratio.

The work done on the system when the crack is introduced is twice the increase in elastic energy, and the surface energy of the crack is

$$W_s = 4 a c \tag{65}$$

per unit thickness of plate. Griffith assumed that, when the potential energy of the external distorting forces is enough to cover the increase of elastic energy and surface energy of a crack increment, the crack will spread. If the crack propagates, the total diminution of the potential energy of the system is:

$$W_e - W_s = \frac{\pi c^2}{E} \sigma^2 - 4 a c \quad . \tag{66}$$

Since the potential energy of the system is being diminished, the system has not yet reached its equilibrium, which is postulated to be a fractured condition. In order to obtain equilibrium, the loss of potential energy of the system must be a maximum, or:

$$\frac{d}{dc} (W_e - W_s) = \frac{2 \pi c}{E} \sigma^2 - 4 \alpha = 0. \tag{67}$$

Solving for the stress σ:

$$\sigma = \sqrt{\frac{2 \alpha E}{\pi c}} \quad , \tag{68}$$

for a thin plate, and, for a thick plate:

$$\sigma = \sqrt{\frac{2 \alpha E}{\pi c (1 - \nu^2)}} \quad . \tag{69}$$

Thus, the value of applied stress needed to achieve equilibrium (fracture) of a body is predicted. Further calculations have shown that assumption of a cleavage-type crack, or an ellipsoidal (penny-shaped) crack, gives values only slightly different from those obtained assuming Griffith's elliptical crack.

Fracture Under Biaxial and Triaxial Stresses. Griffith derived a condition of fracture under biaxial stress directly from the Inglis calculations. The assumption was made that the isotropic material contains cracks, of equal lengths and of equal radii of curvature at their ends, which are oriented randomly. The Inglis solution then gives the maximum stress at the end of the crack having the most dangerous orientation as a function of two principal stresses σ_1 and σ_3. Griffith then assumed that fracture occurs when the maximum local stress present at the end of the most dangerous crack reaches the value of molecular cohesion. These combinations of stresses at which fracture takes place can be expressed by equations in which the only physical constant is the tensile strength for uniaxial stressing (K). These equations represent the fracture criteria for biaxial stressing. If tensile stresses are regarded as positive and $\sigma_1 > \sigma_3$, the fracture criterion is:

if $3 \sigma_1 + \sigma_3 > 0$, fracture occurs when:

$$S_1 = K ; \tag{70}$$

if $3 \sigma_1 + \sigma_3 < 0$, fracture occurs when:

$$(\sigma_1 - \sigma_3)^2 + 8K (\sigma_1 + \sigma_3) = 0. \tag{71}$$

If σ_1 and σ_3 are plotted as rectangular coordinates, Equation (71) is that of a parabola which has its concave side in the direction of the bisector of the negative σ_1 and σ_3 axes; Equation (70) is that of the vertical tangent of this parabola. If all combinations of σ_1 and σ_3 are considered, and not only those for which $\sigma_1 > \sigma_3$, the fracture conditions have to be completed by:

$$\sigma_3 = K , \tag{72}$$

for $3\sigma_3 + \sigma_1 > 0$ when $\sigma_3 > \sigma_1$. This is the horizontal tangent to the same parabola.

According to this criterion, a brittle material can withstand any shear stress, provided a sufficiently high hydrostatic stress is superposed. Equation (71) shows that the hydrostatic pressure needed to prevent fracture at a shear stress $\tau_m = (\sigma_1 - \sigma_3)/2$ is $\tau_m^2/4K$. For uniaxial compression ($\sigma_1 = 0$, $\sigma_3 > 0$), Equation (71) gives the strength as 8K, or the compressive strength in brittle fracture should be eight times the tensile strength. The Griffith biaxial criterion can be applied to triaxial states of stress, since, in the approximations used, normal or shear stress in the plane perpendicular to the edge of the crack cannot exert an appreciable influence.

Number of Flaws. An important question raised by the Griffith theory concerns the number of most effective cracks in the specimen. The scatter of tensile strengths obtained from brittle materials indicates that the number of critically oriented cracks cannot be very large, and generally the strength of a specimen must decrease with size due to the greater probability of its containing a dangerous crack. Griffith found a definite size effect in his experiments on glass fibres. The data are given in Table 1. This size effect could be expressed approximately by Karmarsch's formula:

$$S = A + \frac{B}{d} , \tag{73}$$

where S = the strength,

   A = the strength of large specimens,

   d = the diameter,

   B = a constant.

Holland and Turner[6] used the Karmarsch-Griffith relation to explain variation of breaking strength as a function of width of specimens in bending tests, while Smekal[8] declared that the relationship:

$$S = A_1 - B \log d , \tag{74}$$

gives numerical values which are in as good agreement with experimental data as those of the Griffith form. This relationship has the added advantage of having the same form as the formula which gives the tensile strength as a function of loading velocity v:

$$S = A_2 + B \log v . \tag{75}$$

The strengths obtained from thin fibres by Griffith have been explained in various ways by different investigators. Some of the explanations

TABLE 1. STRENGTH OF GLASS FIBRES, FROM GRIFFITH[7]

Diameter, 0.001 in.	Breaking Stress, psi	Diameter, 0.001 in.	Breaking Stress, psi
40.00	24,900	0.95	117,000
4.20	42,300	0.75	134,000
2.78	50,800	0.70	164,000
2.25	64,100	0.60	185,000
2.00	79,600	0.56	154,000
1.85	88,500	0.50	195,000
1.75	82,600	0.38	232,000
1.40	85,200	0.26	332,000
1.32	99,500	0.165	498,000
1.15	88,700	0.130	491,000

have dealt with the effect of limiting the size of the flaws by the fibre
diameter, some with the decreased probability of containing a "dangerous"
flaw in the very small volume of the fibre, and some with the possibility of
changing molecular structure during the drawing process. However, the
"drawing process" itself seems to suggest the best interpretation of the
phenomenon. The flaws of most dangerous orientation, that is, normal to
the fibre axis, suffer the largest decrease in effectiveness, or may even
be "smeared out". Another theory says that, when the glass is drawn, a
thin surface layer is subjected to compressive stresses which tend to close
any surface flaws. This theory takes on added weight in the light of large
decreases in strength after aging or slight handling of the rods of fibres.
Such treatments might cause a penetration of this thin compressed layer.

Smekal[9], on investigating the fracture surface of circular glass rods
broken in tension, found that a "mirror surface" was formed which had as
its initiation point the critical flaw. Extending from this flaw, the smooth
surface gradually gave way to a rough one. Smekal hypothesized that the
fracture proceeds quite slowly at first, and while so doing creates the mir-
ror surface in a plane normal to the applied stress. As the slow fracture
continues, the tensile stress applied to the remaining portion of the rod in-
creases, owing to the decrease of the effective cross section, and soon
reaches a value which causes flaws of a much less critical nature to begin
to propagate and meet the primary fracture surface in an area of increasing
roughness. At this point, the fracture progresses quite rapidly. From the
rough fracture surface obtained in the rapid-fracture area, it can be de-
duced that the total number of flaws present is quite large.

Temperature Effects. Although at low temperature the effects of rate
of loading and of temperature are small, they become increasingly impor-
tant at higher temperatures. This observation cannot be explained satis-
factorily by elastic theory, and molecular processes must be considered.
If $U*$ is the amount of energy needed to break the molecular bond, the
activation energy, at the flaw edge, and $U (< U*)$ is the elastic energy accu-
mulated due to loading, then at low temperature U must increase to $U*$
before fracture can occur. If the energy of thermal agitation of a bond (ϵ)
is added to the elastic energy due to load (U), the loading of the rod neces-
sary to cause separation of the bond is decreased. However, the separation
of succeeding bonds must await the achievement of a thermal energy $\geq \epsilon$,
so that the process is a slow one compared with bond separation not de-
pendent upon thermal energy. For constant values of loading, the speed of
the primary fracture should depend on the temperature. The rate at which
fracture proceeds depends upon the activation energy $U*$ or the magnitude
of energy required to make the bond unstable, and upon the number of bonds
which possess enough energy to become unstable. The first condition is
self-explanatory; that is, the smaller the activation energy required, the
more rapidly fracture can take place. The second condition depends upon
the distribution of energy in the system. The number of bonds possessing
the required energy can be calculated from the Maxwell-Boltzmann Distri-
bution Law, which states that the number of bonds having an energy greater

than ϵ is proportional to $e^{-U*/RT}$, where the ratio $\dfrac{U*}{RT}$ is the probability factor, and where R is the gas constant and T is the absolute temperature. Then for states requiring large values of thermal energy ϵ and at low temperatures, the probability of obtaining the necessary activation energy is very small. Hence, the probability of fracture's occuring in such a state is small. As the temperature is increased, it can be seen that the probability of fracture increases.

Since fracture, as it is ordinarily thought of, occurred only after a mirror surface, of considerable area in some cases, had been developed, Smekal defined the term the "reduced tensile strength", Z_o, as:

$$Z_o = L/(q - s) \quad ,\qquad\qquad (76)$$

where L = the breaking load,

      q = the total cross-sectional area of the rod,

      s = the area of the mirror surface.

Smekal's tests show that this value, Z_o, is constant, as he had predicted.

Origin of Flaws. Poncelet[10] noted that, while many investigators criticize the prediction of Griffith that a material has a compression strength eight times its tensile strength, the criticisms are not leveled at Griffith's mathematics, but at his postulate that cracks exist in the material in the unstressed state. To circumvent these criticisms, Poncelet hypothesized that the flaws of Griffith (and Smekal) are not present, and proceeded from the "Morse Curve" of atomic physics to a flaw-genesis theory. From this viewpoint, the fraction of bonds, f_o, having a thermal-energy level higher than the energy U* required to rupture a bond between two atoms is:

$$f_o = e^{-U*/kT} \quad ,\qquad\qquad (77)$$

where T = the absolute temperature.

When a tensile force is superposed upon the thermal agitation, the resulting distortion energy ϵ_m increases the fraction of bonds whose atoms have enough energy to break the bond. In a neighborhood of sufficient stress, the number of these "potentially broken bonds" may increase to a density at which a "potential flaw" is formed. The chances that the atoms of the "potentially broken bonds" will form new alliances are considerable and, thus, an actual flaw is formed from a "potential flaw", and stress-concentrating factors are brought into play.

When the material is in compression, the fraction of "potentially broken bonds" at a given stress is much lower than in tension, and a much higher stress must be imposed in order to give equal probabilities of flaw generation. When the flaws are generated before the compressive stress reaches a value of eight times the tensile strength, the Griffith predictions

of relative strengths should hold. In other cases, the flaws will not occur until a higher value of compressive stress is obtained, and higher ratios of compressive to tensile strengths result.

When a fracture is progressing slowly, only the bonds in the plane of the fracture have a high enough stress value to allow an effective probability of bond rupture, and a "mirror surface" is produced. After a reduction in the effective cross-sectional area of a specimen, the stress values at several bonds are high enough to give an effective probability of rupture, and deviating fracture surfaces are formed. This causes the area of increasing roughness surrounding the mirror surface, as found by Smekal.

Weibull's Statistical Theory

Weibull[11] has developed a theory of strength of materials from the elementary laws of statistics, in order to explain the scatter in results obtained experimentally and which could not be explained by the classical theory. If the proposition is allowed that a probability curve exists for the fracture strength of materials, a theory of strength can be developed. Let P be the probability of rupture at a stress σ; then $P = f(\sigma)$. For low values of stress, $P = 0$, and for high values, $P = 1$.

If a given stress is applied to a rod, the probability of the rod's withstanding the load is $1 - P$. When the length of the rod is doubled and the same stress is applied as before, the probability of survival of the system is:

$$1 - P_2 = (1 - P_a)^2 \ , \tag{78}$$

where P_2 = the probability of rupture of the rod of length 2,

$\quad P_a$ = the probability of rupture of the rod of unit length.

From this, it is seen that, for a rod of any length L the general form would be:

$$1 - P_L = (1 - P_a)^L \ , \tag{79}$$

or

$$\log (1 - P_L) = L \log (1 - P_a) \ . \tag{80}$$

Since volume is proportional to length, and if P_o is the probability distribution of the length of rod which corresponds to unit volume:

$$\log (1 - P) = V \log (1 - P_o) \ . \tag{81}$$

If $B = - \log (1 - P)$, called the risk of rupture, it is found to be proportional to the volume and to $\log (1 - P_o)$, which is a function of tensile stress, σ, alone. The risk of rupture of a small element dv is:

$$d B = - \log (1 - P_o) dv \quad , \tag{82}$$

where $\log (1 - P_o)$ is negative because $1 - P_o < 1$.

Therefore:

$$B = \int n(\sigma) dv \quad , \tag{83}$$

for an arbitrary distribution of stresses. The probability of rupture (P) is:

$$P \cong 1 - e^{-B} = 1 - e^{-\int n(\sigma) dv} \quad . \tag{84}$$

This equation expresses the fundamental law of an isotropic brittle material, and the function $n(\sigma)$ expresses the strength of the material. In anisotropic materials, the stress-coordinate system and direction must be taken into account. For cases where fracture always is initiated at the surface, the volume integral may be replaced by a surface integral:

$$\int^V n(\sigma) dv = \int^A n(\sigma) da \quad , \tag{85}$$

or in case separate material functions apply to the surface layer and interior:

$$P = 1 - e^{-\int n_1(\sigma) dv - \int n_2(\sigma) da} \quad . \tag{86}$$

If N measured values are taken, and the distribution curve is obtained from these values, the probability of a single value falling within an increment $d\sigma$ is $\dfrac{dP}{d\sigma} d\sigma$, or the number of values falling within this range is $N\dfrac{dP}{d\sigma} d\sigma$. The ultimate strength σ_b should be then:

$$\sigma_b N = \int_o^\infty \sigma N \frac{dP}{d\sigma} d\sigma \quad , \tag{87}$$

$$\sigma_b = \int_{\sigma=o}^{\sigma=\infty} \sigma dP = \int_o^\infty \sigma de^{-\int n(\sigma) dv} \quad , \tag{88}$$

or, integrating:

$$\sigma_b = \int_o^\infty e^{-\int n(\sigma) dv} d\sigma \quad . \tag{89}$$

The standard deviation a of the value of the ultimate strength may be calculated from the formula:

$$a^2 = \int_0^\infty (\sigma - \sigma_b)^2 \, dP \quad , \tag{90}$$

or:

$$a^2 = \int_0^\infty e^{-\int n(\sigma)dv} d(\sigma^2) - \sigma_b^2 \quad . \tag{91}$$

The assumption has been made in the foregoing derivations that σ is a one-dimensional tensile stress; therefore, it is scalar if the risk of rupture is independent of stress direction. If there are arbitrarily distributed forces, then σ is to be replaced by another scalar which is determined by the principal stresses, and this reduced stress may be used in the above derivations. In other words, each combination of principal stresses requires the use of a specific material function.

The material function $n(\sigma)$ is included in the above derivations. If the function is defined by:

$$n(\sigma) = k\left(\frac{\sigma}{\sigma_o}\right)^m \quad , \tag{92}$$

where σ_o is the strength determined from classical theory, $\frac{P}{A}$, and m is a constant which increases with perfection of the body. If m increases toward infinity, the probability curve becomes discontinuous at the point $\sigma = \sigma_o$, where it jumps from 0 to 1. The ultimate stress is then:

$$\sigma_b = \int_0^\infty e^{-\int n(\sigma)dv} \approx \int_0^{\sigma_o} d\sigma = \sigma_o \quad , \tag{93}$$

and the variance a^2 is:

$$a^2 = \int_0^\infty e^{-\int n(\sigma)dv} d(\sigma^2) - \sigma_b^2 = \int_0^{\sigma_o} d(\sigma^2) - \sigma_o^2 = 0. \tag{94}$$

These two equations define the classical theory of strength, and show it to be a special case of the general statistical theory. The factor σ_o is seen to be the classical strength of the material, and the variance is equal to zero, the basis on which the classical theory is regarded as untenable in light of experimental scatter in results.

Since one of the basic assumptions of the general statistical theory was the existence of a probability curve which was a function of stress

only, the material function $n(\sigma)$ is the crux of the theory and, while the theory cannot be applied unless some specialization of the function is made, the specific form of the function to be used in a particular stress system is the result of assumption and, hence, a possible source of error. Weibull found that, in the light of limited experimental data, good agreement could be obtained by letting the material function be defined as:

$$n(\sigma) = K\sigma^m \quad , \tag{95}$$

where K and m are constants.

If $K = \dfrac{1}{\sigma_o^m}$, the probability of rupture for volume V will be:

$$P = 1 - e^{-V(\sigma/\sigma_o)^m} \quad , \tag{96}$$

so that, for volume $V = 1$ and the stress σ equal to the classical strength σ_o, the probability of rupture is 0.63. The "risk of rupture" in tension is given thus as:

$$B = V\left(\frac{\sigma}{\sigma_o}\right)^m \quad . \tag{97}$$

The ultimate strength can be expressed as:

$$\sigma_b = \frac{\sigma_o}{V^{1/m}} \int_o^\infty e^{-Z^m} \, dZ \quad , \tag{98}$$

where $Z = \dfrac{\sigma}{\sigma_o} V^{1/m}$,

or, letting $I_m = \displaystyle\int_o^\infty e^{-Z^m} \, dZ$,

$$\sigma_b = \frac{I_m \, \sigma_o}{V^{1/m}} \quad , \tag{99}$$

and the variance (a^2) is:

$$a^2 = \int_Z^\infty e^{-V(\sigma/\sigma_o)^m} \, d(\sigma^2) - \sigma_b^2 \quad , \tag{100}$$

or,
$$a^2 = \frac{\sigma_o^2}{V^{2/m}} \left[I_{m/2} - I_m^2 \right] \quad . \tag{101}$$

From the above equations, it may be seen that the ultimate strength and standard deviation decrease with volume increases. That the ratios of variance to strength are independent of volume and dependent upon the exponent m may be seen from:

$$\frac{a^2}{\sigma_b^2} = \frac{I_{m/2}}{I_m^2} - 1 \quad . \tag{102}$$

Polyaxial Stresses. In reconsidering the one-dimensional stress case, it is assumed that compressive stresses have no effect on the risk of rupture, and the principal stress is located in the direction of the x axis. The normal stresses which are included in the small spatial angle $d\theta$ contribute to the risk of rupture B an amount $n_1(\sigma) \, d\theta$, and, where the integration is carried over half the surface of the sphere:

$$B = \int_0^{\pi/2} n(\sigma) \cdot 2\pi \sin\phi \, d\phi = -2\pi \int_0^1 n_1 \left(\sigma_1 \cos^2\phi \right) d\cos\phi \quad , \tag{103}$$

or, if $n_1 = K_1 \sigma^m$:

$$B = \frac{2\pi}{2m+1} K_1 \sigma^m \quad . \tag{104}$$

If $n = K\sigma_1^m$, for a one-dimensional stress:

$$K_1 = \frac{2m+1}{2\pi} \cdot K \quad . \tag{105}$$

If σ_1 and σ_3 are the principal stresses, the normal stress σ_n is, from Figure 2, for the two-dimensional case:

$$\sigma_n = \cos^2\phi \left(\sigma_1 \cos^2\psi + \sigma_3 \sin^2\psi \right) \quad , \tag{106}$$

and
$$d\theta = \cos\phi \, d\psi \, d\phi \, . \tag{107}$$

The risk of rupture is then

$$B = 2K_1 \int_0^{\pi/2} \int_{-\psi_o}^{+\psi_o} \cos^{(2m+1)}\phi \left(\sigma_1 \cos^2\psi + \sigma_3 \sin^2\phi \right)^m d\phi \, d\psi \, . \tag{108}$$
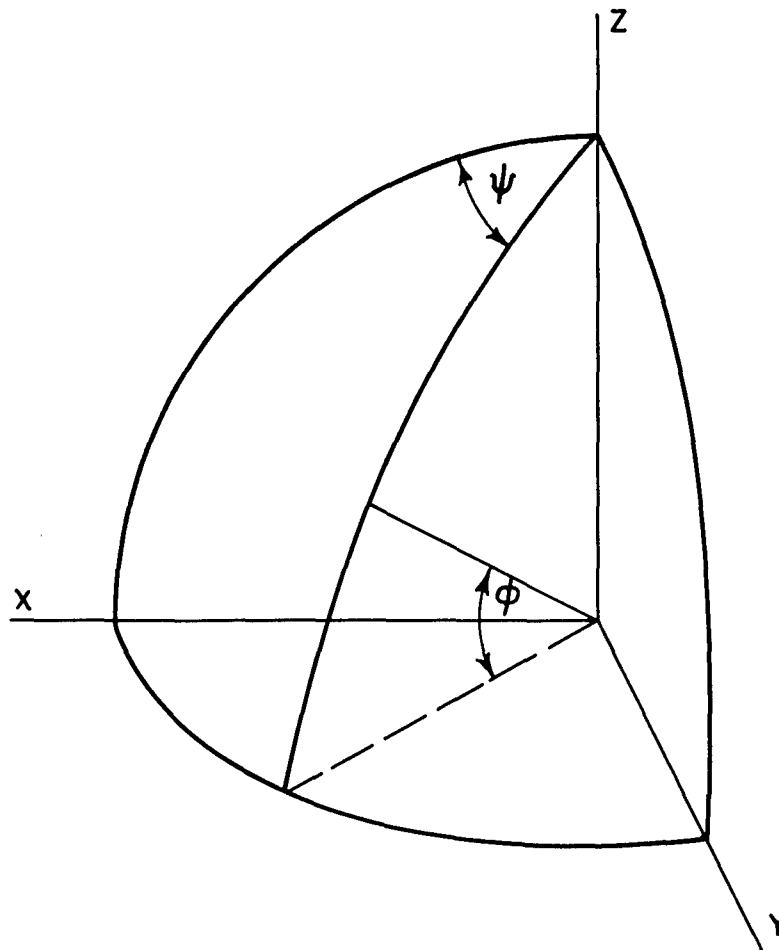
FIGURE 2. STRESS DIAGRAM

This equation can be solved for various combinations of σ_1 and σ_3. In the case of shear:

$$\tan \psi_0 = \sqrt{\frac{\sigma_1}{-\sigma_3}} = -1 \; , \tag{109}$$

where:

$$\psi_0 = \pi/4 \quad . \tag{110}$$

Substituting this value of ψ_0 into Equation (110), the risk of rupture for shear becomes:

$$B = 2 K_1 \sigma_1^{\,m} \int_0^{\pi/2} \cos^{(2m+1)}\phi \, d\phi \int_0^{\pi/2} \cos^n \theta \, d\theta \quad . \tag{111}$$

For a three-dimensional stress, $\sigma_1 = \sigma_3 = \sigma_2$, the normal stress is independent of the direction and the risk of rupture is:

$$B = (2m + 1) K \sigma_1^{\,m} . \tag{112}$$

Bending. The risk of rupture of a rectangular beam subjected to pure bending is:

$$B = \frac{V}{2(m+1)} \left(\frac{\sigma_b}{\sigma_0}\right)^m \; , \tag{113}$$

or, since the risk of rupture in tension is $B = V \left(\dfrac{\sigma_t}{\sigma_0}\right)^m$, the ratio of bending to tensile strengths is:

$$\frac{\sigma_b}{\sigma_t} = (2m + 2)^{1/m} \quad . \tag{114}$$

Torsion. For a circular rod, the risk of rupture is:

$$B = \frac{2}{m+2} V K_2 \, \tau_m^{\,m} \; , \tag{115}$$

where τ_m = the maximum shearing stress.

<u>Tucker's Modification.</u> Tucker[12] agreed with the Weibull analysis only in part. Where Weibull assumed a "weakest link" hypothesis in the development of his theory, Tucker said another method should be postulated to interpret properly some of the experimental data which he obtained. The weakest link theory, as the name implies, proposes that a specimen composed of a single link (or small volume) will have a higher mean strength than one composed of many links or elements. The standard deviation from the mean strength of the single-link specimens also will be larger.

Values of the mean strength and standard deviation of strengths of chains as a function of number of links, as developed by Tippett[13], were applied by Tucker to changes of length of specimens in tension, compression, torsion, and bending, and to changes of depth of beams in bending. Tucker proposed another theory, the strength-summation theory, to explain changes in strength with changes in the cross-sectional area of specimens. Here, the strength of the material was assumed to be independent of the change in area, while the standard deviation, a, of the strength of the material varied according to the equation:

$$k = a_1 / a_A ,\tag{116}$$

where a_A = standard deviation of specimen of cross-sectional area A,

and a_1 = standard deviation of unit area.

A new combination theory was offered by Tucker. In this theory, the calculation of strength is the same as for the weakest link theory, but the calculation of standard deviation of strength is defined by the term $k_1/\sqrt{n}$, where k_1 is the standard deviation of a unit element, and n is the number of elements. The predictions of modulus of rupture of a beam in bending given by the three theories of strength are summarized below, with Hooke's Law assumed to apply until fracture:

Theory of Failure	Modulus of Rupture, psi
Classical maximum stress	400
Weakest link	470 ± 35
Combination	590 ± 120

The results obtained for the modulus of rupture from the combination theory are approximately of the magnitude that Tucker estimated they should be, and were in good agreement with his test results.

Frankel[14] discussed the general statistical theory, and the analyses of Weibull and Tucker in particular. Since Frankel was interested largely

in explaining the increase of modulus of rupture in beams in bending over tensile strength, he derived Weibull's equations to that end, and listed values of the constant K in the following equation for different types of loading:

$$P = 1 - e^{-K V \left(\frac{\sigma - \sigma_e}{\sigma_o}\right)^m}, \tag{117}$$

where P = the probability of rupture,

σ_e = lowest possible strength of specimen,

σ_o = classical tensile strength (constant - see Equation 96),

m = material function (constant).

The results for beams under various test conditions are given in Table 2. From this table, the modulus of rupture will be smaller for third-point or sixth-point loadings than for center-point loadings. Frankel also showed that Tucker used a normal curve, in an attempt to avoid the specialization of the probability curve that Weibull assumed. Not only did Tucker end with an equation of exactly the same form as Weibull, but his hypothesis is a specialization of Weibull's, when $m = 2$.

TABLE 2. VALUES OF K FROM FRANKEL'S ANALYSIS

Type of Loading	K
Pure bending	$\dfrac{1}{2(m+1)}$
Center-point loading	$\dfrac{1}{2(m+1)^2}$
Third-point loading	$\dfrac{2}{3}\left[\dfrac{1}{2(m+1)^2}\right] + \dfrac{1}{3}\left[\dfrac{1}{2(m+1)}\right]$
Sixth-point loading	$\dfrac{1}{3}\left[\dfrac{1}{2(m+1)^2}\right] + \dfrac{2}{3}\left[\dfrac{1}{2(m+1)}\right]$

Theory of Rate Processes as Applied
to Brittle Fracture

Background. The phenomenological and mechanistic theories of
strength suffer from one important defect. The variable, time, which
cannot be separated from the conduct of any critical test of a stressed body,
is not considered. In short, these theories do not consider the effect of
rate of loading or the possible effect of the length of time in which a body
remains at a certain stress level. Experimental evidence is available which
indicates a distinct effect of these two factors on the fracture of brittle ma-
terials.

A discussion has been included here on the theory of rate processes
and on how this theory can be applied to brittle materials to give a more
complete understanding of the phenomena of fracture. As such, this theory
is not a theory of fracture, but rather a theory of rate processes.

The theory is based primarily on the suggestions by S. Arrhenius[15]
that an equilibrium exists between inert and active molecules of a reactant,
and that only the active molecules can take part in the reaction or process.
The general equation expressing the variation of the specific rate of a proc-
ess with the temperature is:

$$r = A \exp(-E/RT) \ , \tag{118}$$

where E = the difference in heat content between the activated and the inert
　　　molecules,
　　A = a quantity that is independent, or varies relatively little, of
　　　temperature,
　　R = the gas constant,
　　T = the absolute temperature,
　　r = the rate of the process.

More recently, using the tools of quantum and statistical mechanics[16],
the theory of reaction rates has been advanced to a state which describes
most of the phenomena observed in nature. The end product of the theory
will be utilized in this discussion, as the derivation of basic relations is
lengthy and complex. If a material proceeds from State A to State B by the
addition of some external energy, an equilibrium between States A and B
occurs during this change. In other words, there is at any time an equilib-
rium between the amounts of A going to B and the amounts of B going to A.
This is given simply by the relation:

$$K^* = r_1/r_2 \ , \tag{119}$$

where K^* = equilibrium constant,
　　r_1 = the rate of A going to B,
　　r_2 = the rate of B going to A.

The over-all rate of the process is given by the relation:

$$r = \frac{kT}{h} K^* ,$$

(120)

where k = Boltzmann's constant,
      h = Planck's constant,
      T = the absolute temperature,
      r = the rate of the process.

The factor $\frac{kT}{h}$ is a frequency factor, and represents the frequency with which the activated complexes proceed to completion of the reaction. This is represented graphically in Figure 3.
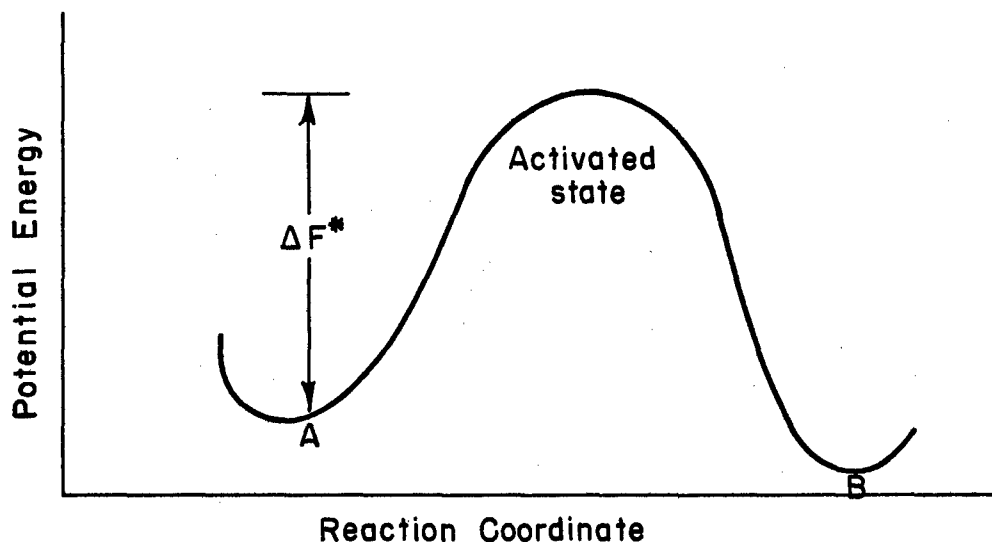

FIGURE 3. POTENTIAL BARRIER FOR A RATE PROCESS

A-2187

Therefore, any complex from A which reaches the top of the energy barrier proceeds to State B with a frequency of $\frac{kT}{h}$.

Borrowing from thermodynamics, it is known that the equilibrium constant K^* may be expressed in terms of the free energy of the process as:

$$K^* = \exp(-\Delta F^*/RT) ,$$

(121)

where ΔF^* = the free energy of activation.

ΔF^* represents the difference in energy between State A and the activated state. Equation (120) can be rewritten then as:

$$r = \frac{kT}{h} \exp(-\Delta F^*/RT) \quad . \tag{122}$$

It is often convenient to use the energy and entropy of activation, rather than the free energy. This is done by remembering from thermodynamics that:

$$\Delta F^* = \Delta H^* - T \cdot \Delta S^*$$
$$= E - T \cdot \Delta S^* + RT \quad , \tag{123}$$

where ΔH^* = heat of activation,
ΔS^* = entropy of activation,
E = energy of activation.

Equation (122) can be rewritten then in the form:

$$r = \frac{ekT}{h} \exp(-E/RT) \exp(\Delta S^*/R) \quad . \tag{124}$$

The entropy of activation ΔS^* has some physical significance. It is related to the probability of occurrence of the initial and activated states, excluding the energy difference, or what may be called the relative freedoms of the two states. A negative value of ΔS^*, therefore, means that the activated state involves greater restrictions on the degrees of freedom of the molecules than the initial state.

Another operation which is performed commonly, as will be seen later in this section, is the addition of several free energies of activation. In this case, Equation (122) can be written as:

$$r = \frac{kT}{h} \exp(-\Delta F_1^*/RT) \exp(-\Delta F_2^*/RT) \exp(-\Delta F_3^*/RT) \quad . \tag{125}$$

For example, some of the energy required to reach the top of the energy barrier may come from heat, some from stress, some from an electrical field, etc. This background forms the basis for all modern thinking, and all the theories to be discussed can be resolved simply to the form of Equation (125).

Application to Fracture Phenomena. Machlin and Nowick[17], in their treatment of stress rupture of metals, take account of the addition of an external stress field to the free energy of activation required for a process. If a stress, such as shear stress r, is applied, it may lower the barrier in one direction and raise it in the opposite direction by an amount Br, as

shown by the dashed curve of Figure 4. The activation energies for the two directions are no longer equal, and the process takes place with a definite net rate.

Reaction Coordinate
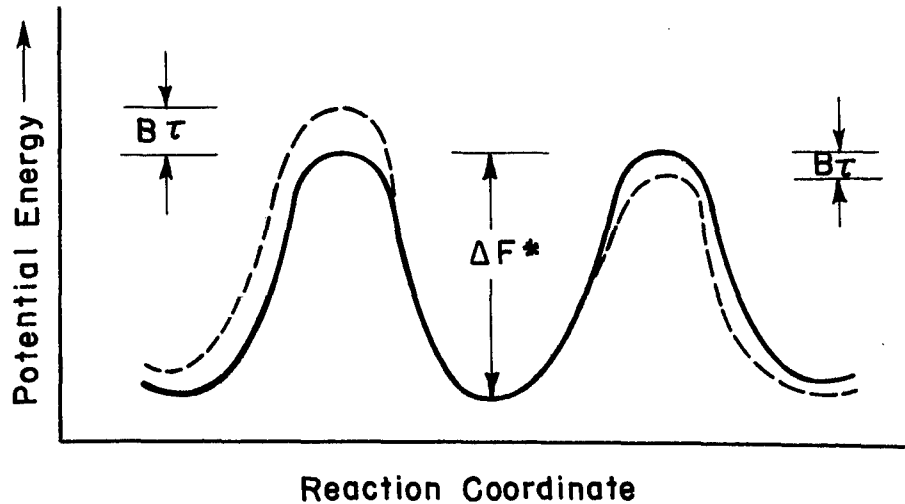
FIGURE 4. POTENTIAL BARRIER FOR A STRESS-DEPENDENT RATE PROCESS

A-2188

The rate of occurrence in the positive direction can be expressed as:

$$r^+ = (kT/h) \exp\left[-(\Delta F^* - B\tau)/kT\right] \quad ,$$

and in the negative direction as:

$$r^- = (kT/h) \exp\left[-(\Delta F^* + B\tau)/kT\right] \quad .$$

The net rate is then:

$$r = r^+ - r^- = (2kT/h) \exp\left[-\Delta F^*/kT\right] \sinh(B\tau/kT) . \qquad (126)$$

Equation (126) describes the rate of a process which is stress dependent, such as crack propagation, plastic flow, or creep phenomena.

Cutler and Gibbs[18] follow a similar line of reasoning in their development of an expression for a net rate for the fracture of glass. They assume that the superposed potential is a linear function of the applied stress in the neighborhood of the barrier. ΔF^* in Equation (122) may be replaced then by

$\Delta F_1^* - L_1(x)(\sigma - \sigma_o)$, where ΔF_1^* is the average height of the barrier when no stress is present, and σ is the value of the stress calculated from the theory of elasticity for a homogeneous isotropic medium. σ_o is that value of σ for which the final state has free energy equal to that of the initial state. $L_1(x)$ is the lowering of the barrier per unit of applied stress; it accounts for the effective "area" of the moving atom, the concentration of stress due to the finite crack of length x, and the discontinuous nature of matter on an atomic scale.

At equilibrium, particles also pass from right to left across the barrier (bonds mending). For this occurrence, the barrier has a height of $\Delta F^* = \Delta F_1^* + L_2(x)(\sigma - \sigma_o)$, where $L_2(x)$ has properties analogous to those of $L_1(x)$, and accounts for the asymmetry of the potential-energy curve.

The net rate of bonds broken when $\sigma > \sigma_o$ is then:

$$r_{net} = \frac{kT}{h} \exp\left(-\frac{\Delta F^*}{RT}\right)\left\{ \exp\left[\frac{L_1(x)(\sigma - \sigma_o)}{RT}\right] - \exp\left[-\frac{L_2(x)(\sigma - \sigma_o)}{RT}\right]\right\}. \quad (127)$$

When $\sigma < \sigma_o$, the net rate is zero.

Cutler and Gibbs subsequently determine the velocity of crack propagation from Equation (127). If w is the average increase in length of a crack accompanying separation of one pair of atoms, and x is the length of the crack, dx/dt would be the velocity. It is given for $\sigma > \sigma_o$ by:

$$dx/dt = w r_{net} = \frac{wkT}{h} \exp\left(-\Delta F^* /RT\right)\left\{ \exp\left[\frac{L_1(x)(\sigma - \sigma_o)}{RT}\right]\right.$$
$$\left. - \exp - \left[\frac{L_2(x)(\sigma - \sigma_o)}{RT}\right]\right\}. \quad (128)$$

From Equation (128), it is seen that each crack is characterized by a set of quantities w, ΔF^*, and σ_o, and the functions $L_1(x)$ and $L_2(x)$. These quantities may vary from crack to crack. The L functions depend on the shape and size of the crack and on its orientation with respect to the principal stress. The stress at the tip of a crack increases as the crack length increases. Therefore, the stress-concentration factors $L_1(x)$ and $L_2(x)$ are increasing rapidly, direct functions of the crack length x, which increases with time. When testing is done with a steadily increasing load, the applied stress is proportional to the time, so that the crack length increases with the stress. For this condition, the L functions can be considered strong direct functions of the applied stress.

A plot of dx/dt versus σ would have the form as shown in Figure 5. To the left of σ_o, the value of dx/dt is zero because the initial state is one
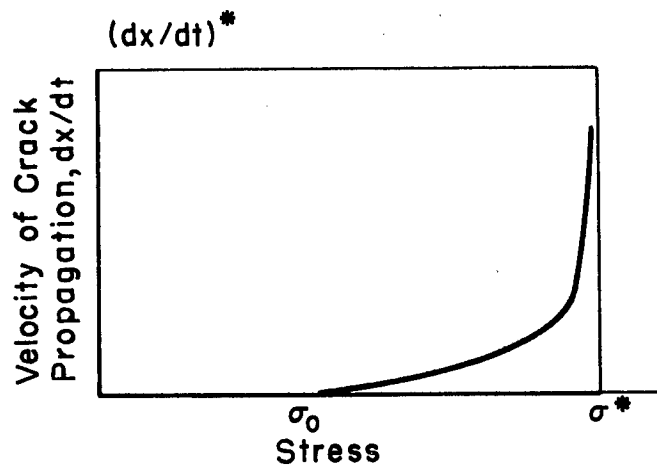
FIGURE 5. A PLOT OF THE VELOCITY OF CRACK
PROPAGATION AS A FUNCTION OF STRESS

A- 2189

of lower energy than the final state. To the right of σ_0, dx/dt would have
the general form of a hyperbolic-sine function of $L_1 = L_2 = $ a constant.
Owing to the dependencies of the L functions on σ, the "break" in the curve
will be somewhat sharper than a true hyperbolic-sine curve. At very low
rates of increase of σ, the L's may be considered to be independent of
$d\sigma/dt$ and T.

Qualitatively, fracture might occur either when the propagation rate
reaches an arbitrary critical value or when the crack reaches a certain
critical length. In effect, these two criteria are equivalent, since, once
started, fracture will be completed in an extremely short time.

Fracture can be defined then as occurring when dx/dt reaches a cer-
tain critical value (dx/dt)*. According to Equation (128), this corresponds
to σ's having a critical value σ^*. Owing to uncertainty in knowing just
when fracture occurs, σ^* is not defined precisely. The dx/dt-versus-σ
curve is so steep in the region of σ^*, however, that the resulting uncertainty
of σ^* is very small in comparison with the magnitude of σ^*. Thus, σ^* has
a specific value which is almost independent of the definition of fracture,
and each flaw is characterized by a critical value of the stress. When the
applied stress equals or exceeds this critical value σ^*, fracture results.

Several other workers, such as Cox[19] and Poncelet[10,20], have used the rate-process theory in studying the strength of glass. Nearly all of the published data concern different types of tests, so caution must be used in comparing the equations and results obtained. The two articles by Poncelet describe efforts to understand the crushing of glass and the so-called static fatigue. These articles have been reviewed, but their content is not considered to be of importance at this time. It must be said that Poncelet's viewpoints are contrary to the opinion expressed by the majority of investigators and, as such, require critical examination. This does not mean to imply that there are no good thoughts in his writings, but, since reaction-rate principles are not utilized in the sense of this review, a discussion of his papers will be deferred. The article by Cox was considered vague because of the large number of arbitrary constants involved in his formulations. A worth-while future effort might be an attempt to simplify his analysis.

Saibel[21], using thermodynamics, has arrived at an expression for the velocity of crack propagation which is similar to that of Machlin and Nowick, and of Cutler and Gibbs. The basic Eyring equation for the rate of a process is used in the form:

$$r = \frac{2\lambda kT}{h} \exp(-\Delta F*/RT) \sinh \frac{w}{kT} , \tag{129}$$

where λ = the distance through which the unit of flow moves in one jump,
  w = the work done to move the unit of flow.

The unit of flow in Saibel's theory is a hole, and a crack propagates by the continuous formation of holes. By assuming that the work w to form the holes is equal to the heat of activation for the process, then:

$$\frac{w}{kT} = n\Delta H*/RT , \tag{130}$$

where k = R/N = gas constant/Avogadro's number,
  n = N/n_h = Avogadro's number/number of holes per mol.

Equation (129) can be rewritten now as:

$$r = \frac{2\lambda kT}{h} \exp(-\Delta F*/RT) \sinh \frac{n\Delta H*}{RT} . \tag{131}$$

Saibel assumes further that $\Delta H*$ is given adequately by the relation:

$$\Delta H* = L_m \Delta V/V + p , \tag{132}$$

where L_m = the latent heat of melting,
  ΔV = the change in volume on passing from solid to liquid state,
  V = the molecular volume of the solid at the melting point,
  p = the hydrostatic component of the force acting at the point of formation of a hole.

Equation (132) allows the rate of crack propagation to be calculated adequately from existing data. This is facilitated by remembering that $\Delta F^* = \Delta H^* - T \cdot \Delta S^*$, and by assuming that the solid is a random mixture of atoms and holes. The entropy is given then as the entropy of mixing, and is described by the relation:

$$\Delta S^* = NR \left[(1 + c) \ln (1 + c) - c \ln c \right] \quad ,$$

where $c = 1/n$, and varies from 0.3 to 0.5. Saibel's theory has proved to be rather sound, and calculations based on his theory have checked well with measurements of fracture velocity in metals.

Correlation of Treatments of the Rate-Process Theory. Three theories have been reviewed in detail. All of them are modifications of Eyring's basic reaction-rate theory. It is interesting to compare them for possible correlation of the stress-dependent term. For convenience, the equations are rewritten below.

Machlin and Nowick:

$$r = 2 \, kT/h \, \exp (-\Delta F^*/kT) \, \sinh (B_r /kT) \, ; \tag{126}$$

Cutler and Gibbs, assuming $L_1(x) = L_2(x)$:

$$r = dx/dt = \frac{wkT}{h} \, \exp (-\Delta F^*/RT) \, \sinh \left[\frac{L_1(x)}{kT} (\sigma - \sigma_0) \right] \, ; \tag{128}$$

Saibel:

$$r = \frac{2\lambda kT}{h} \, \exp (-\Delta F^*/RT) \, \sinh \frac{n\Delta H^*}{kT} \, . \tag{131}$$

Since $k = R/N$, there is no essential difference between the exponential terms of the three equations. From examination, it is possible, at least qualitatively, to make the following comparison for fracture:

$$B_r \sim L_1(x) \, (\sigma - \sigma_0) \sim n\Delta H^* \quad .$$

It should be remembered that Saibel's theory applies to a state of stable crack propagation, and the other two allow for stresses less than the critical stress required to form a stable crack. If the comparison is made for the same conditions, the similarity becomes even more striking:

$$B'\sigma_c \sim L(x) \, (\sigma_c - \sigma_0) \sim n\Delta H^* \quad ,$$

where $\sigma_c = 2_r$.

The conclusions apparent from this discussion are: (1) there are a number of ways to express this same relation, and (2) the theory of reaction rates can be a powerful tool in describing brittle fracture, if properly used and interpreted.

A need for data to check the validity of the three theories is evident. The effects of strain rate or stress rate and of temperature should be studied, and better understanding of these effects should do much to clarify the thinking on the brittle-fracture problem.

This survey shows how the principle of the rate-process theory can be applied to the fracture strength of brittle solids. The parameters that are obtained describe the strength of a material more completely than is possible if the factor of time is not considered.

From the practical point of view, tests should be conducted with the rate of loading as a controlled variable. Data from such tests can be used to obtain parameters which describe the behavior of a material much more completely than merely stating that the material has a strength of x pounds per square inch.

EXPERIMENTAL WORK

The previous laboratory work on this project and the preceding review of theories indicated that a flaw-type mechanism offered the most likely basis for developing the desired correlations in strength properties of a ceramic material. Most of the experimental work covered by the present report was guided accordingly.

An interpretation of fracture phenomena on the basis of a flaw-type mechanism appears to require consideration of three elements: (1) the theoretical strength; (2) the stress-concentration factor of the critical flaw; and (3) the probability of a flaw with this stress-concentration factor initiating fracture. Of these three elements, the latter was most attractive for study in the initial experimental program. According to theory, the probability element is a statistical function of the number of flaws, and, hence, of the effective volume under stress. Also, in Weibull's treatment, a theoretical background exists for such work. Finally, valuable engineering formulae might result, as evidence exists of the significant effect of this element on fracture strength.

Such an experimental program reduces to isolating the effect of size on strength. In addition, several incidental experiments were conducted during the past year, for such purposes as checking materials and perfecting tests.

Materials

The selection of suitable materials for investigation has been one of the more difficult aspects of this project. As pointed out earlier, reproducibility from specimen to specimen is essential. The material also must be representative of a ceramic material and, as a large number of rather complex specimens are needed, fabricability and cost are important factors.

An ideal material has not been found. During the year, most of the work was with plaster of Paris. Some additional experiments were conducted with the same material as used last year, K151A, a commercial titanium carbide product. Also, preliminary tests were made using a spark-plug porcelain. Details of each material follow.

Plaster

Two types of plaster of Paris were used, Hydrocal and Hydrostone. Both are products of the United States Gypsum Company. Specimens were made by casting to shape in appropriate Perma-Flex* molds.

The Hydrocal batch was prepared by first adding 300 grams of Hydrocal to 143 grams of distilled water. The two components were mixed slowly in a kitchen-type mixer, taking care to eliminate bubbles from the mix. The resulting slurry was poured slowly into the molds so as not to entrap air. After the plaster had set (about 40 minutes), the specimens were removed from the mold and cured for 12 days in the normal atmosphere of the laboratory.

Hydrostone specimens were prepared by adding 1500 grams of the powder to 550 grams of distilled water, and mixing slowly for one minute in a kitchen-type mixer. Then a bell jar was placed over the mixer, and mixing continued for five minutes with the bell jar evacuated to about 1 inch of mercury absolute. Specimens were removed from the molds about 30 minutes after the plaster had set, and were cured at room temperature for 15 hours. Finally, the specimens were cured in a dryer at 110 F until the 14th day after casting, when they were tested.

Hydrostone has proven to be the more suitable of the two plasters because of its greater hardness and strength. Plaster specimens are inexpensive and fabricated easily; however, their properties are not reproduced easily, being sensitive to slight changes in conditions of preparation and curing. Nevertheless, with careful control, plaster has proven to be a fairly reliable material.

---

*Perma-Flex Cold Molding Compound, Perma-Flex Mold Company, Columbus, Ohio.

K151A

K151A is a nickel-titanium carbide product of Kennametal, Incorporated, with a nickel content of 20 per cent and a specific gravity of 5.8. All of the specimens of this material were fabricated by Kennametal.

During the course of the investigation, it was found that K151A has two undesirable characteristics for present use on this project. It exhibited slight plastic flow prior to fracture, thus complicating any analysis of fracture behavior. Also, K151A was not suitably reproducible from specimen to specimen. Defects often were readily discernible in the material and, in several cases, fracture appeared to originate at one of the defects. This problem with K151A was brought out earlier, in AF Technical Report No. 6512.

Originally it was planned to try to use K151A specimens that had been shaped prior to final sintering. Sufficiently close tolerances were not obtained by this method on tension and torsion specimens. Accordingly, most of the tension and torsion specimens tested this year were machined after final sintering. The type of surface is indicated in the appropriate section describing the experimental work.

Porcelain

The porcelain specimens were obtained from Champion Spark Plug Company. They were made of a high-alumina, spark-plug porcelain, unglazed. This material is felt to represent a very carefully controlled ceramic product, and the initial tests indicated a desirable degree of uniformity among specimens.

Methods

Data were obtained from room-temperature bend, tension, and torsion tests. Details of these tests were given previously, in AF Technical Report No. 6512. Some modifications were necessary in connection with the experiments, such as changes in specimen design for size-effect studies. Each modification is described later, in the section devoted to the particular experiment. In addition, since the elimination of test variables is essential to meeting the objectives, work was done directly on the development and refinement of test methods. This work is covered independently later, under 'Development and Refinement of Tests".

Effect of Size on Strength

In these experiments, an attempt was made to isolate the effect of gage-section size on strength. Briefly, the picture created by mechanistic theories is that the measured stress is an average stress. The actual stress over the cross section is nonuniform, with stress peaks existing in minute volumes as the result of stress concentrations from flaws or defects. Fracture occurs when the average (measured) stress is increased to a level where one of the stress peaks becomes equal to the theoretical strength. When the size of the gage section is increased, a larger number of stress peaks will be present. If the distribution of flaws is amenable to statistical laws, the increased population of peaks is more likely to contain one of greater magnitude. From this, it is predicted that both measured strength and standard deviation will decrease as the gage-section size is increased.

Preliminary Experiments

Bend tests were made on Hydrocal specimens of two different sizes, as follows:

Nominal	Gage-Section Dimensions, in.		
Size	Depth	Breadth	Length
Large	3/8	1-1/2	2-1/8
Small	3/8	1/4	5/8

The spans between points of load application and support were as follows:

	Span, in.	
Size	Supports	Load
Large	6-3/4	4-3/4
Small	5	3

The load was applied in 2- and 10-pound increments for the small and large specimens, respectively, with approximately a one-minute interval between each successive loading step. Stress was calculated in the usual manner, from the equation $\sigma = \frac{Mc}{I}$. The following data were obtained:

Size	Average Strength, psi	Standard Deviation, psi	No. of Specimens
Large	1045	45	4
Small	1365	55	5

Similar experiments were conducted on K151A specimens of three sizes, as follows:

Nominal Specimen Size	Gage-Section Dimensions, in.		
	Depth	Breadth	Length
Large	0.375	0.625	0.625
Medium	0.300	0.500	0.500
Small	0.225	0.375	0.375

The load was applied in 200-pound increments to specimens of each size, with sufficient time between load applications to permit strain-gage readings to be taken. The spans between points of load application and of support were as follows:

Size	Span, in.	
	Supports	Load
Large	5	3
Medium	4-1/4	2-1/4
Small	3-3/16	1-11/16

The resulting data* were:

Size	Average Strength, psi	Standard Deviation, psi	No. of Specimens
Large	102,800	3,300	5
Medium	120,500	14,120	5
Small	135,000	13,810	6

In both of these experiments, the average strength increased with decreases in size, in qualitative accord with theory. Also, in each case, except for the medium and small K151A specimens, the standard deviation increased with size decreases, as theory predicts.

Young's-modulus measurements were made on K151A specimens to indicate whether material or testing variables had any influence. Young's modulus, as a function of gross stress, rather than stress peaks, is expected to be independent of size, and variations with size might be attributed to uncontrolled variables. Values taken from two specimens each of the medium and small specimens were:

Size	Young's Modulus, 10^6 psi	
	Tension	Compression
Medium	72.7	80.0
	54.2	78.6
Small	61.9	59.7
	64.3	57.7

---

* Data for the large-size specimens were taken from AF Technical Report No. 6512. Young's moduli in tension and compression were considered equal in computing strengths of the medium and small specimens.

The average values for the large specimens, from AF Technical Report No. 6512, were 55.1 x 10^6 and 57.7 x 10^6 psi, in tension and compression, respectively. A few scattered inclusions of a foreign material were observed in the fracture faces of the specimens for these measurements. Their strengths were mostly quite low, with a large scatter in individual values, as might be expected, and were discarded. However, the values of Young's modulus were fairly consistent; it is doubtful whether the inclusions had any appreciable influence on either scatter or the average values. The following data* were recorded, indicating little variation with size:

	Tension			Compression		
Size	Average	Standard Deviation	No. of Specimens	Average	Standard Deviation	No. of Specimens
Large	55.1	2.2	9	57.7	7.0	9
Medium	57.6	4.0	5	59.6	3.5	3
Small	55.5	4.4	5	55.7	4.1	5

Young's Modulus, 10^6 psi

These preliminary experiments are considered adequate to conclude that size effects cannot be ignored in developing even a working knowledge of strength in ceramic materials. The data also afford some qualitative support for the statistical treatments of the flaw-type mechanism of fracture.

Attempts to supplement these bend tests with data on size effect from tension tests did not produce acceptable data. It was concluded that a redesign of the tensile specimen would be necessary.

Individual Effects of Gage-Section Length, Breadth, and Depth on Bend Strength

To record more details of the size-effect phenomena, an extensive program of bend tests was conducted on Hydrostone specimens with the length, depth, or breadth of the gage-section as the controlled variable. These data are considered necessary for a quantitative understanding of strength properties from different tests. Questions existed on such matters as whether length and periphery effects are the same, whether internal and external flaws are equally critical, and whether the slope of the stress gradient in a bend or torsion specimen has any influence on the fracture strength in each case.

Table 3 gives the gage-section dimensions of the specimens tested. The load was applied in increments, with approximately a one-minute interval between each successive loading step. The load increment for each specimen size also is given in Table 3. Stress at fracture was calculated

---

* Data for the large-size specimen were taken from AF Technical Report No. 6512.

TABLE 3. DETAILS OF BEND TESTS ON HYDROSTONE SPECIMENS OF VARIOUS SIZES

Specimen Size No.	Gage-Section Dimensions, in.			Loading Increment, lb	Span, in.	
	Depth	Breadth	Length		Load Points	Support Points
1	3/8	5/8	5/8	5	3	5
2	3/8	5/8	1	5	3-3/8	5-3/8
3	3/8	5/8	1-1/2	5	3-7/8	5-7/8
4	3/8	5/8	2	5	4-3/8	6-3/8
5	3/8	5/8	2-1/2	5	4-7/8	6-7/8
6	3/8	1/4	5/8	5	3	5
7	3/8	5/8	5/8	5	3	5
8	3/8	1	5/8	10	3	5
9	3/8	1-1/4	5/8	10	3	5
10	3/8	1-1/2	5/8	10	3	5
19	3/8	2-1/2	5/8	10	3	5
11	1/4	5/8	5/8	5	3	5
12	3/8	5/8	5/8	5	3	5
13	1/2	5/8	5/8	10	3	5
14	5/8	5/8	5/8	20	3	5
15	3/4	5/8	5/8	20	3	5

from the conventional formula, $\sigma = \dfrac{Mc}{I}$, which assumes equal Young's moduli in tension and in compression. The spans between points of load application and of support were adjusted for the changes in specimen size and are listed for each size in Table 3.

Strength data on each size except No. 19 were obtained from two lots of Hydrostone specimens, designated Lots A and B. No known variables existed between the two lots. However, Lot A was prepared and tested first, and it is felt that the experience gained probably contributed to better control for the fabrication and testing of Lot B.

Data from each lot are recorded separately in Table 4. The data are plotted in Figures 6, 7, and 8 to show the individual effects of changes in gage-section length, breadth, or depth on the observed strength values of each lot.

TABLE 4. STRENGTH OF HYDROSTONE BEND SPECIMENS OF VARIOUS SIZES

| Specimen Size No. | Gage-Section Dimensions, in. | | | Lot A | | | Lot B | | |
	Depth	Breadth	Length	Average Strength, psi	No. of Specimens Tested	Standard Deviation, psi	Average Strength, psi	No. of Specimens Tested	Standard Deviation, psi
1	3/8	5/8	5/8	2190	15	210	1980	10	160
2	3/8	5/8	1	2160	16	150	1930	15	250
3	3/8	5/8	1-1/2	2060	13	180	1870	17	110
4	3/8	5/8	2	2000	17	180	1860	18	160
5	3/8	5/8	2-1/2	1980	17	160	1690	17	70
6	3/8	1/4	5/8	1990	13	130	2030	13	150
7	3/8	5/8	5/8	2190	15	210	1980	10	160
8	3/8	1	5/8	2050	9	120	1900	14	180
9	3/8	1-1/4	5/8	2010	13	130	1830	14	180
10	3/8	1-1/2	5/8	2010	14	150	1770	14	180
19	3/8	2-1/2	5/8	--	0	--	1600	16	140
11	1/4	5/8	5/8	1910	10	150	1910	16	240
12	3/8	5/8	5/8	2190	16	210	1980	10	160
13	1/2	5/8	5/8	2180	13	220	2100	14	230
14	5/8	5/8	5/8	2250	14	180	2140	10	140
15	3/4	5/8	5/8	2130	9	190	2160	10	210

It will be noted in Figures 7 and 8 that Lot B exhibited a more consistent strength change than did Lot A, supporting the thought expressed previously that conditions were better controlled throughout the experiments on Lot B. Recalling that no known variables existed between the two lots, the differences in their average strengths, evident in each of the figures indicate some ineffectiveness in controlling all significant variables between the two lots.
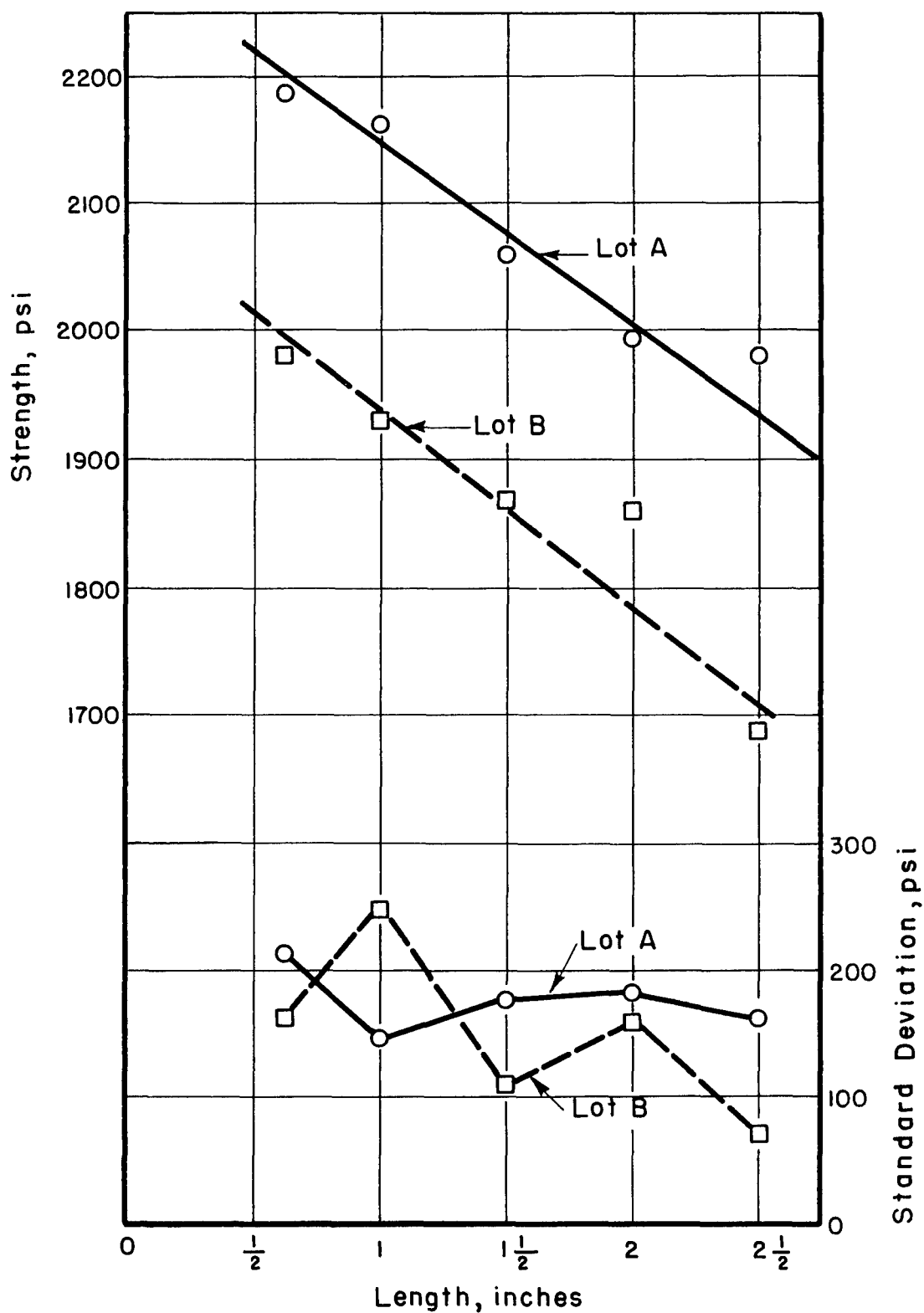
FIGURE 6. AVERAGE STRENGTH AND STANDARD DEVIATION
OF HYDROSTONE BEND SPECIMENS WITH
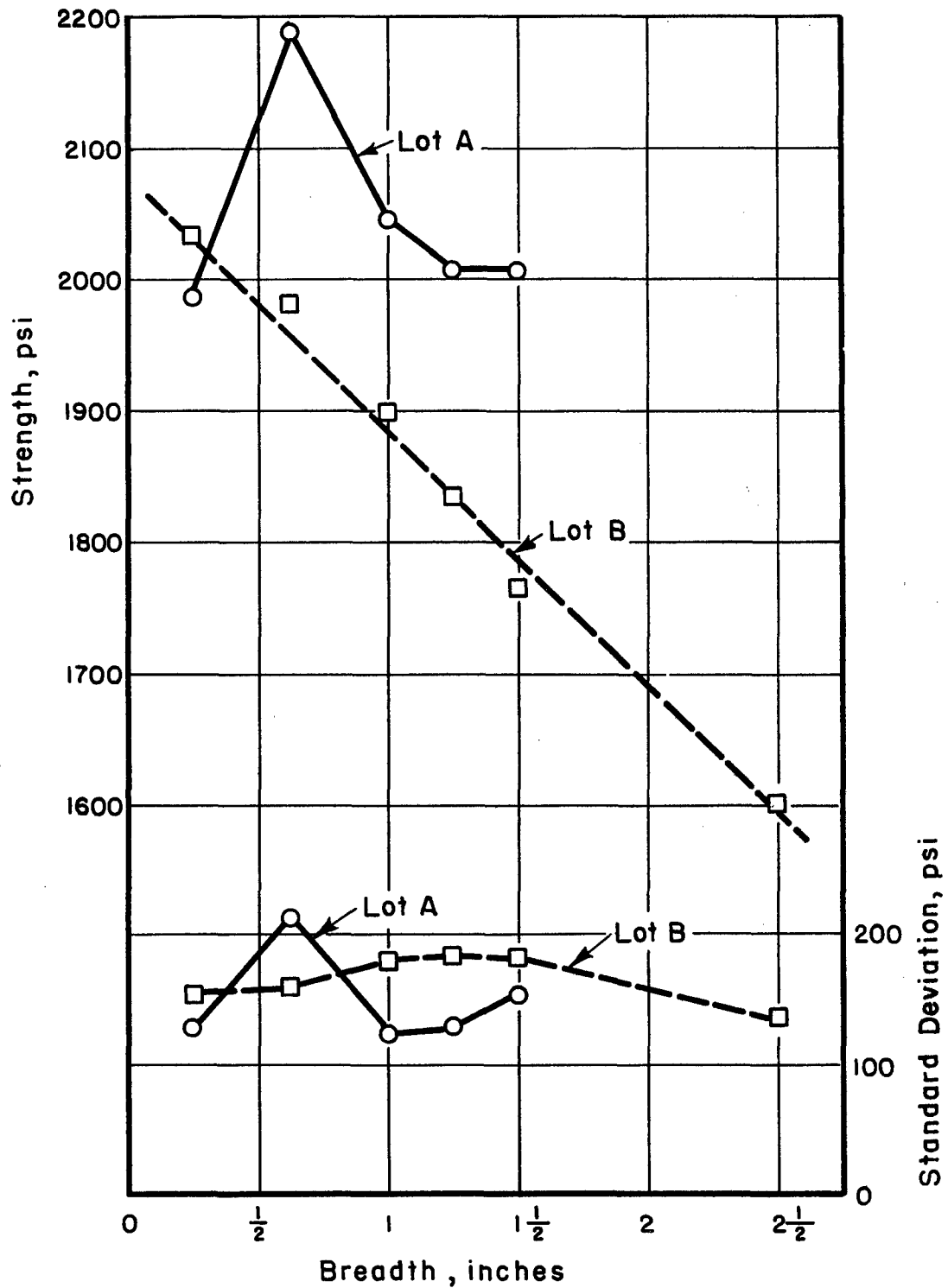VARIOUS GAGE-SECTION LENGTHS

FIGURE 7. AVERAGE STRENGTH AND STANDARD DEVIATION
OF HYDROSTONE BEND SPECIMENS WITH
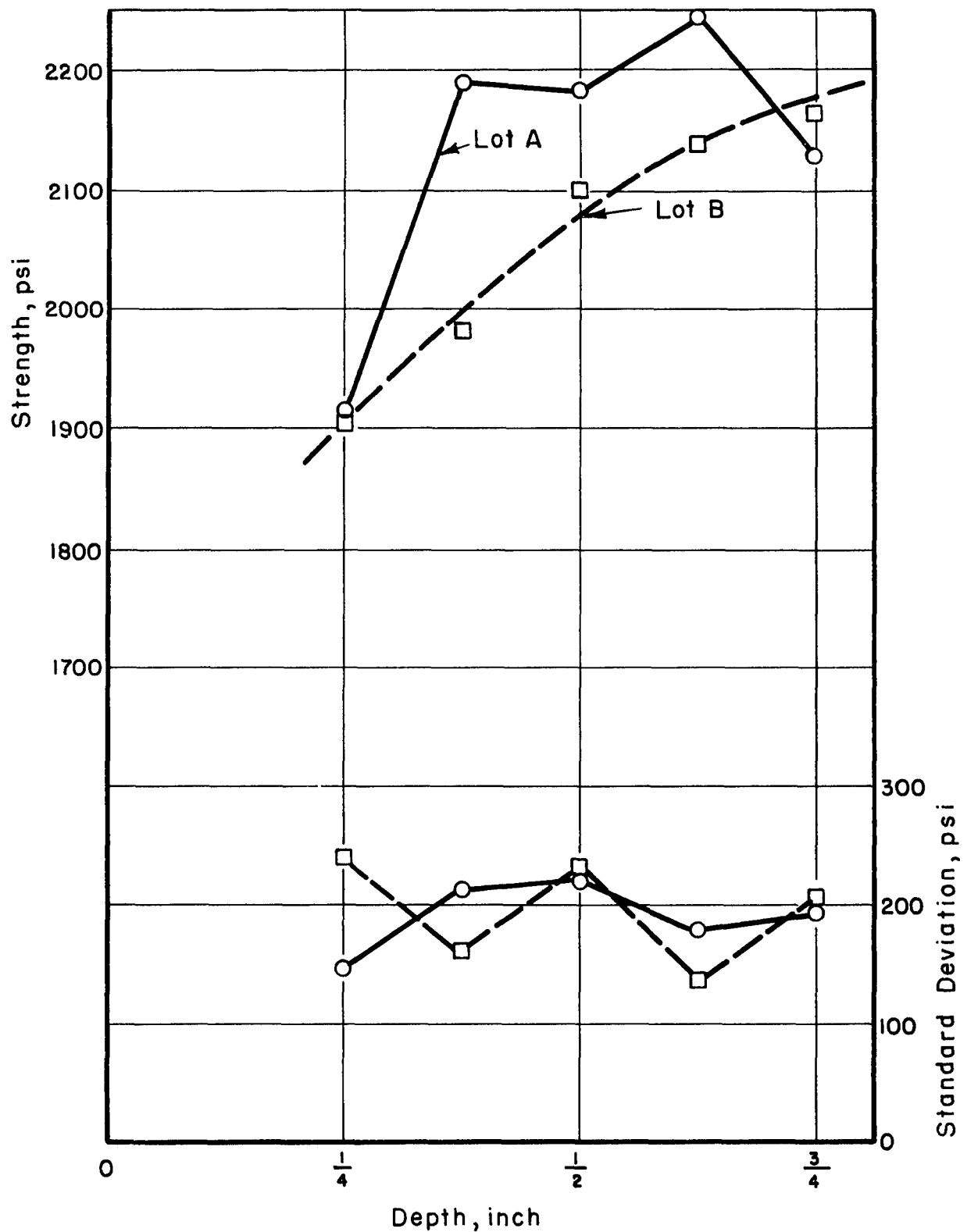VARIOUS GAGE-SECTION BREADTHS

FIGURE 8. AVERAGE STRENGTH AND STANDARD DEVIATION
OF HYDROSTONE BEND SPECIMENS WITH
VARIOUS GAGE- SECTION DEPTHS

A-2192

In general, the changes in standard deviation with the individual changes in gage-section length, depth, or breadth were inconsistent, and the over-all trend indicates little or no size dependence of standard devia- tion. This might indicate that statistics are not involved in the observed size effect on strength. Standard-deviation values for a greater range of dimensions should be obtained to establish better the effect, if any.

A possible exception to these generalizations was the variation in Lot B of standard deviation with gage-section length (Figure 6). In this case, there is a somewhat indistinct trend towards lower deviations with increased lengths, in qualitative agreement with statistical theory.

The changes in average strength were consistent and pronounced with each change in gage-section dimension for Lot B, and with changes in gage- section length for Lot A. Also, the relationship between length and strength was the same for Lots A and B. Although, the data were rather incon- sistent, the breadth-strength and depth-strength trends for Lot A were of the same general nature as those for Lot B. From these facts, one might conclude that strength is size dependent, or that a size-dependent variable was not accounted for in the experiments.

Average strengths decreased linearly with increases in gage-section length. The decrease was at the rate of about 150 psi per inch, or roughly 7-1/2 per cent per inch. The strength also decreased linearly with in- creases in gage-section breadth, at the rate of about 190 psi per inch or 9-1/2 per cent per inch. Such decreases in strength with increases in size agree qualitatively with theoretical expectations from a flaw-type mechanism of fracture. Contrary to any known theory, however, average strength in- creased with increases in gage-section depth. This increase was more pronounced than either the length or the breadth effect on strength, within the limits of the tests. However, the strength-depth curve was nonlinear, with a progressively decreasing slope.

Changes in gage-section depth alone do not change the number of sur- face flaws under maximum tension in a bend test. If only these flaws can be critical, one would not have expected any depth effect in these experiments. This would be the limiting case, according to theory. If internal flaws can be critical, their number would be increased by increases in depth and, theoretically, strength would decrease. Hence, in view of the anomalous behavior in the strength-depth experiments, a size-dependent uncontrolled variable is indicated as an influence in the observed size effects on strength, and the statistical probability of the number of flaws is not wholly involved.

Some consideration can be given to the possibility of such uncontrolled variables at this point. Both gross material variables and extraneous stresses could be size dependent. If gross material variables were influ- ential, one would not have expected the slope of the strength-depth curve in Figure 8 to be opposite that of the strength-length or strength-breadth curves in Figures 6 and 7. In other words, a change in any dimension

would be expected to have the same type of effect. Two sources of extraneous stresses appear to be the most likely possibilities: (1) those from the stress concentration near the points of load application, and (2) those from friction at the supports and at the points of load application.

Unfortunately, present knowledge is inadequate for treating these possible superposed stresses rigorously. However, some approximations might be made as to changes in their significance with the dimensional changes. From Duckworth's analysis of bending[22], a compression stress would be superposed on the critical tension stress in the bottom fibers of the bend specimens by the stress concentrations near the loading points. The special specimen design used in these tests was developed with attention to eliminating any significant influence of this superposed stress. If this provision were ineffective, it would appear, from an approximate expression, that the superposed stress would have no influence on the observed changes in strength with breadth (Figure 7). However, it might be expected to cause a decrease in strength with the increases in gage-section length, if fracture always occurred at midspan where the critical tension stress would be greatest with this superposed stress present. From this, the stress concentration near the loading points does not appear to explain the breadth effect, and any error from this source would cause the difference in slope between the strength-breadth and the strength-length curves to be opposite from that observed. It might be concluded tentatively, therefore, that the observed strength-dimension phenomena did not result from this superposed stress. The nature of this possible effect on the length-depth data involves too many assumptions for any meaningful conclusion.

An analysis of the effect of friction on bend-test data is given later in the report. The effect of any superposed stress from this source appears to be a function of the depth and the moment arm, if one assumes that movement occurs and the frictional coefficient is the same at all contacts. On this basis, the nature of the change in strength with length or breadth would be independent of friction forces. The error from these forces, if present, would be constant in both cases. However, any superposed stress from friction would be expected to cause the observed strength to increase with increases in gage-section depth. Friction, therefore, might account for the anomalous behavior in the strength-depth experiments.

Although this analysis has been speculative and qualitative of necessity, the indications are that the observed breadth and length effects on bend strength are the result of a real size dependence on strength, and the observed depth effect might be influenced by error in determining the actual stress at fracture. The analysis establishes rather conclusively that effort should be made to determine whether testing variables influenced these data before considering them acceptable for use in developing fracture relationships. Such an effort was made through Young's-modulus determinations.

As pointed out earlier, Young's modulus, as a function of gross stress, rather than a stress peak, is expected to be independent of size. Any variation in Young's modulus with size, therefore, might be attributed to a change in the material or to a size-dependent error in determining stress.

In the experiments on Lot A, spot determinations were made of Young's modulus, with no evidence of a size dependence, as follows:

Specimen Size No.	Gage-Section Dimensions, in.			Average Young's Modulus, 10^6 psi		No. of Specimens Tested
	Depth	Breadth	Length	Tension	Compression	
1	3/8	5/8	5/8	2.52	2.68	5
5	3/8	5/8	2-1/2	2.54	2.59	3
11	1/4	5/8	5/8	2.57	2.74	3
12	3/8	5/8	5/8	2.52	2.68	5
15	3/4	5/8	5/8	2.47	-	2

After obtaining the more acceptable strength data from Lot B, these moduli values from Lot A were considered of questionable significance. Additional experiments were conducted.

Using the same conditions as those used to obtain the strength data in Table 4, the moduli of specimens with two gage-section depths were measured. The specimens were prepared from a new lot of Hydrostone, designated Lot C. Results were as follows:

Specimen Size No.	Gage-Section Dimensions, in.			Average Young's Modulus, 10^6 psi		No. of Specimens Tested
	Depth	Breadth	Length	Tension	Compression	
11	1/4	5/8	5/8	2.30	2.44	5
15	3/4	5/8	5/8	2.54	2.76	5

On the basis of these data, a size-dependent material variable or extraneous stress was present, and the strength-depth data in Table 4 were influenced in a manner which would tend to cause the observed strength to increase with depth increases.

A similar experiment was made, except that gage-section breadth was varied, and a fourth lot of Hydrostone specimens, Lot D, was used. The data were as follows:

Specimen Size No.	Gage-Section Dimensions, in.			Average Young's Modulus, 10^6 psi		No. of Specimens Tested
	Depth	Breadth	Length	Tension	Compression	
7	3/8	5/8	5/8	2.75	2.45	3
10	3/8	1-1/2	5/8	2.52	2.38	3

These results afford further evidence that the strength-dimension data in Table 4 were influenced by a variable other than a real size dependence of strength. As in the case of depth changes, the observed trend in strength with breadth changes is the same as would be expected if only this extraneous variable were acting.

There is an apparent contradiction here of the previous analysis of possible error from size-dependent variables. The analysis indicated that no size-dependent gross material variable was present, and that the breadth effect should not be influenced by any superposed extraneous stress. In view of this contradiction, another breadth-modulus experiment was made as a check, using Lot E. The results were as follows:

Specimen Size No.	Gage-Section Dimensions, in.			Average Young's Modulus, 10^6 psi		No. of Specimens Tested
	Depth	Breadth	Length	Tension	Compression	
7	3/8	5/8	5/8	2.52	2.88	4
9	3/8	1-1/4	5/8	2.50	2.67	4

These data tend to upset the contradiction and, in support of the analysis, indicate that superposed stress did not influence the strength-breadth data in Table 4. The following results of a check breadth-modulus experiment, using still another lot of Hydrostone specimens, Lot F, added further support:

Specimen Size No.	Gage-Section Dimensions, in.			Average Young's Modulus, 10^6 psi		No. of Specimens Tested
	Depth	Breadth	Length	Tension	Compression	
7	3/8	5/8	5/8	2.62	2.41	4
10	3/8	1-1/2	5/8	2.65	2.47	2

It is of probable significance that, in these two similar experiments, the observed compression modulus was greater than the tension modulus with Lot E and less than the tension modulus with Lot F. As there is no known reason for a true difference between compression and tension moduli, the observed difference might be attributed logically to the presence of extraneous stresses. It follows that any change in this difference would be from a change in the relative magnitudes of the resultant stresses superposed on the tension and compression fibers.

In an effort to learn more about the nature of the apparent superposed stress, using Lot F, another depth-modulus experiment was made. Specimens were used with longer gage sections and with loading points moved farther from the gage section than in the previous modulus-dimension experiments. Both of these provisions would reduce any possible error from stress concentrations at the loading points. Also, the moment arm was adjusted so that the load would produce a given stress which was more nearly constant for each depth. Specific details of the experimental conditions were as follows:

Specimen Size No.	Gage-Section Dimensions, in.			Span, in.	
	Depth	Breadth	Length	Load Points	Support Points
21	1/4	5/8	1	3-1/2	5-1/2
20	1	5/8	1	3-1/2	7-1/2

The results were surprising:

Specimen Size No.	Average, Young's modulus, 10^6 psi		No. of Specimens Tested
	Tension	Compression	
21	2.72	2.47	3
20	2.17	1.97	4

Here, modulus decreased with the increase in depth, the effect being opposite that in the previous depth-modulus experiments and opposite that expected from the trend in depth-strength data in Figure 8. The following strength measurements show that this trend also was reversed by the change in conditions:

Specimen Size No.	Average Strength, psi	No. of Specimens Tested
21	1790	10
20	1520	10

Over all, these modulus experiments show that the strength-depth data obtained by the present bend-test technique are influenced markedly by testing variables. Unless a means is developed to treat these variables rigorously, the data in Figure 10 are of no value in contributing to an understanding of the effect of size on brittle fracture. The implications from this finding, along with the lack of consistent variations in standard deviation with length or breadth changes, the finding in Lot D of a breadth effect on modulus, and the inconsistent differences between tension and compression moduli in breadth-moduli experiments introduce doubt concerning the safe use of the strength-length or strength-breadth data. This doubt is offset by the speculations on the effect of likely extraneous stresses, and by the experimental findings of no appreciable breadth effect on moduli in Lots E and F.

It is essential that this subject of size effect be pursued further to meet the objectives of this project. In so doing, it appears necessary to obtain bend-test data in which the influence of extraneous stresses is known to be absent, and additional attention needs to be given to the possible source of such stresses. The previous speculations, and the experimental finding of a pronounced depth effect in Lot F, where special provisions had been taken to reduce any effect from stress concentrations at the loading point, indicate friction as the source. The observed inconsistencies in

moduli behavior also indicate friction as the source of the extraneous stress. It is well known that friction coefficients can be quite erratic; hence, the friction force concomitant with any movement at contacts could vary greatly. Without movement, the forces tending to produce movement also are complex. Two factors enter here, the tension or compression strains and the deflection. On the compression side of the specimen, the compression strain and the deflection tend to produce movement in the same direction, but on the tension side, they oppose each other. Therefore, a number of effects are possible.

It is concluded, therefore, that extraneous stresses from friction were the principal source of the observed testing variables. The acceptance of the strength-length and strength-breadth data in Figures 6 and 7 as true effects of size on strength should await further examination of the influence of this testing variable.

It should be mentioned that, if friction is the source of error, the effect probably would be more pronounced in plaster than in fired ceramic bodies, whether movement occurred or not. Plaster, being softer, would have a higher frictional coefficient and, having a lower modulus, would have a greater force tending to produce movement.

Effect of Type of Test

As mentioned earlier, an extensive program of testing was conducted last year on K151A. Elastic and strength data were obtained from bend, tension, torsion, and compression tests. The objective of this work was primarily to establish the effect of the type of test on mechanical-property data, in the interests of developing relationships in the mechanical behavior of ceramics. Secondary interests were in the actual properties of K151A, because of its potential utility in aircraft engines, and in evaluating the various tests for use in the development of ceramic bodies.

This work is covered in AF Technical Report No. 6512. For convenient reference, the data obtained have been taken from this report and are included here in Table 5.

The testing of K151A was continued during the period of the present report. Additional torsion tests were conducted; bend tests were made with center-point loading; the stresses in previous bend tests were recalculated considering the effect of observed plastic flow in K151A; and the possible error from friction in the bend test was studied.

TABLE 5. MECHANICAL-PROPERTY TESTS OF K151A*

	Bend Test	Tension Test	Compression Test	Torsion Test
Average strength, psi	102,800	55,100	407,400	80,000
Standard deviation, psi	3,300	6,750	23,300	-
Number of specimens tested	5	6	5	3
Average Young's modulus in tension, 10^6 psi	55.1	53.9	-	-
Standard deviation, 10^6 psi	2.2	1.0	-	-
Number of specimens tested	9	6	-	-
Average Young's modulus in compression, 10^6 psi	57.7	-	54.2	-
Standard deviation, 10^6 psi	7.0	-	1.6	-
Number of specimens tested	9	-	6	-
Average modulus of rigidity, 10^6 psi	-	-	-	23.2
Number of specimens tested	-	-	-	3
Average Poisson's ratio in tension	0.21	0.25	-	-
Standard deviation	0.02	-	-	-
Number of specimens tested	9	2	-	-
Average Poisson's ratio in compressions	0.22	-	0.22	-
Standard deviation	0.02	-	0.01	-
Number of specimens tested	7	-	4	-

* From AF Technical Report No. 6512.

Torsion Tests

The data in Table 5 were supplemented this year by additional room-temperature torsion tests on K151A.

In the first series of additional tests, four of the five specimens were loaded by torque increments of about 60 inch-pounds (2500 psi), rather than continuously, as in the previous torsion tests. The torque was held constant after each applied increment while twist readings were made. This loading procedure more closely approximates that which was used in the bend, tension, and compression tests on K151A.

The results from this series, along with results of all earlier torsion tests, are given in Table 6. Values for strength were calculated both from the elastic formula, used in the past:

$$r = \frac{2T}{\pi r^3} \quad , \tag{133}$$

and from the expression which takes into account deviations from Hooke's Law:

$$r = \frac{1}{2\pi r^3} \left(\theta \frac{dT}{d\theta} + 3T \right) \quad , \tag{134}$$

where r = shear stress, psi,
   T = torque, in.-lb,
   r = specimen radius, in.,
   θ = twist of specimen, radians per in.

As in the previous torsion tests, flaws were observed in the fracture faces of each torsion specimen in this series. Fracture apparently was initiated at one of these flaws in each case. Also, some bending was observed in checks on two specimens of this series, even though particular attention was given to adjusting the grips and remachining parts to obtain close alignment. The specimens also were checked closely and found to be free of warpage. The bending was indicated by strain measurements, made in the manner described in AF Technical Report No. 6512.

Within the limits of these experiments, the change to incremental loading appeared to lower the strength and proportional limit without appreciably affecting the modulus of rigidity.

For the next series of torsion tests, the twisometer was refined for increased accuracy, and a new torque-measuring device was used to eliminate a slight drift observed in the cantilever beam used previously. These changes are described later under "Development and Refinement of Tests". Also, the specimens were machined to obtain closer tolerances than were

TABLE 6.   TORSION TESTS ON K151A WITH CONTINUOUS
AND INCREMENTAL LOADING

Specimen No.	Type of Loading	Modulus of Rigidity, 10^6 psi	Strength, psi		Proportional Limit, psi
			Elastic	Plastic	
1-1*	Continuous	23.8	74,900	74,900	53,500
1-3*	Continuous	21.4	69,600	58,400	63,000
1-4*	Continuous	24.3	95,500	95,500	59,000
1-9	Continuous	21.0	79,100	70,900	50,000
1-5	Incremental	21.6	70,000	67,000	39,000
1-7	Incremental	-	67,000	-	-
1-8	Incremental	24.2	52,600	51,600	29,000
1-10	Incremental	-	72,000	-	-

Note: No strain measurements were obtained on Specimens 7 and 10 owing
to malfunctioning of the twisometer.
* Data on these specimens from AF Technical Report No. 6512.

obtained in the "as-sintered" specimens used in earlier work. Continuous, rather than incremental, loading was used.

Table 7 presents the resulting values of strength, calculated from the elastic formula, Equation (133), and of modulus of rigidity. The shear stress-strain curves from this series were all practically straight lines, making any choice of a proportional limit questionable and the use of the plastic expression for stress unnecessary. Qualitative checks indicated no bending in the tests.

TABLE 7. RESULTS OF REFINED TORSION TESTS

Specimen No.	Modulus of Rigidity, 10^6 psi	Strength, psi
2-2	23.7	82,500*
2-3	24.2	100,100
2-4	22.0	104,700
2-6	22.5	103,500*
2-7	22.2	96,500
2-8	22.2	105,300
2-9	22.1	98,000*
2-10	23.7	90,500*
2-11	22.1	99,000
Average	22.7	97,800
Standard Deviation	1.7	6,930

* Flaws were observed in the fracture faces of these specimens.

The average modulus of rigidity from this series, 22.7×10^6 psi, is lower than that recorded in Table 5, 23.2×10^6 psi, and more closely agrees with the values calculated from Young's modulus and Poisson's ratio from the tension and compression tests assuming isotropy, 21.3×10^6 and 22.0×10^6 psi, respectively.

The average strength in Table 7 was lowered somewhat by including those specimens having obvious flaws in their fracture faces. Disregarding these flawed specimens, the remaining five specimens have an average strength of 101,100 psi with a standard deviation of 3,400 psi. Of particular interest is the fact that, for all practical purposes, this is the same strength and standard deviation as obtained from the bend test, recorded as 102,800 psi with a standard deviation of 3,300 psi. No flaws were observed in the

bend-test specimens used to obtain these values. Earlier, with less refined torsion tests on porous and nonporous porcelain, reported in RAND Report R-209, the torsion strength was one-half the bend strength.

Certain reasons exist to expect the same strengths in torsion and bend tests, as observed here, if the tests are precise. The torsion speci- mens all fractured with a helical break about 45° to the specimen axis. This fracture is normal to the axis of the maximum tension component, indi- cating that tension stress rather than the shear stress was critical. This tension stress would be equal to the shear stress. Bend-test specimens also fractured in tension. Furthermore, in both tests the tension stress was a maximum at the surface and decreased to zero at the specimen axis. From this, one might conclude that, with adequate refinements, bend and torsion tests yield equal strength values.

However, the distinct possibility exists that the observed equality between torsion and bend tests was coincidental. Factors to be considered include:

1. The torsion tests were made on specimens with machined surfaces, using continuous loading, as opposed to "as- sintered" surfaces and incremental loading for the bend tests. Table 6 indicates that the two types of loading might give somewhat different strengths. Although no truly com- parative data exist, the higher strength in these torsion tests than in earlier ones might be owing to the change in surface, rather than the testing refinements and freedom from flaws in the material.

2. There is a compression stress normal and equal to the tension stress in the torsion test, while only a uniaxial tension acts on the critical region in bend tests. Some theories predict different strengths under uniaxial and biaxial stress systems.

3. Evidence exists of error, probably from friction, in the bend test; however, this error probably is within the limits of practical consideration of the equality in bend and torsion tests from data at hand.

4. The pronounced size effect observed earlier in tests on plaster must be taken into account before any positive conclusion on the ratio of torsion and bend strengths is possible.

Future work on this project is expected to resolve these questions. Meanwhile, the torsion tests have furnished valuable and interesting data in guiding such work.

Bend Tests With Center-Point Loading

Strength and Young's modulus values were determined on K151A with the bend test modified. Rather than applying two equal loads at symmetrically located points outside the reduced gage section, as was done earlier to obtain the bend-test data in Table 5, a single load was applied at midspan. The specimen design, span, method of loading and supporting, and other features of the test method were unchanged.

With the modification, the test represents that commonly used in ceramic practice, and the data obtained were intended for use in establishing the effect of type of bend test. Several factors appear to be involved in this simple change, including:

1. On the basis of a flaw-type mechanism of fracture, a higher fracture strength would be expected with center-point loading because of the reduced size of the "gage section".

2. A greater superposed compression from the stress concentration near the applied load would be expected with center-point loading, making the apparent fracture strength and Young's modulus higher.

3. Any friction effects would be less with center-point loading, causing the apparent fracture strength and Young's modulus to be lowered.

4. Center-point loading does not permit placing a resistance strain gage on the top (compression) fibers, and any difference between compression and tension moduli in the material cannot be taken into account, without a new method of strain measurement.

5. With center-point loading, a gage on the bottom surface measures strain over a gage length, rather than at the point where maximum strain occurs. For this reason, the actual strain is probably greater than the measured strain, causing the observed value of Young's modulus to be high.

The initial tests with center-point loading were made on a different lot of K151A bend specimens than was used to obtain the data in Table 5. The results were as follows:

Specimen No.	Strength, psi	Young's Modulus, 10^6 psi
1	92,900	55.0
2	73,100	54.5
3	95,900	55.3
Average	87,300	54.9

This average strength, 87,300 psi, is considerably below that found with two-point loading, 102,800 psi. An opposite effect was obtained earlier in tests of a porcelain, reported in RAND Report R-209. In these earlier tests, center-point loading yielded higher strength values. A microscopic examination of the K151A specimens used for the present comparison tests showed distinct material variations. Surface cracks perpendicular to the specimen axis were observed on the specimens used in the tests with center-point loading, but not on those tested with two-point loading. These cracks undoubtedly lowered the strength, and the data are not considered suitable for comparing the two tests.

To extend this effort, three K151A bend specimens from the same lot as those used to obtain the data in Table 5 were fractured with center-point loading. Two of these specimens, K-OB-9 and K-OB-10, had been stressed previously to about 70,000 psi. The data obtained were:

Specimen No.	Strength, psi
K-OB-9	96,100
K-OB-10	95,000
K-OB-11	98,600
Average	96,800

Although these strengths are still less than the average from tests with two-point loading, 102,800 psi, and fail to confirm the trend found in porcelain, they show rather conclusively that material variations influenced the earlier comparison on K151A. The previous stress history appears to have lowered the strength of Specimens K-OB-9 and K-OB-10, making further comparison tests necessary for acceptable data. Over all, it is apparent that present knowledge of fracture and testing variables is inadequate for generalizations on relative strength values from the two bend tests.

Plastic Bending of K151A
_____

To date, calculations of stress from bend-test data have assumed that the material obeyed Hooke's Law. This assumption, of course, is invalid for K151A, which exhibited a proportional limit. Recently, the method described by Nadai[23] was used to account for the deviations from Hooke's Law in correcting the strength values obtained from the bend tests on K151A recorded in AF Technical Report No. 6512.

According to Nadai, the outer fiber stresses in a rectangular bar under pure bending can be expressed as:

$$\frac{\sigma_t \sigma_c}{\sigma_t + \sigma_c} = \frac{1}{bh^2 \phi} \frac{d(M\phi^2)}{d\phi} , \qquad (135)$$

where σ_t, σ_c = unit stresses in outer tension and compression fibers, respectively,

   b = breadth of gage section,

   h = depth of gage section,

   M = external moment,

   ϕ = slope of the tangent to the neutral axis.

Equation (135) reduces to:

$$\frac{\sigma_t \sigma_c}{\sigma_t + \sigma_c} = \frac{1}{bh^2} \left(2M + \frac{\phi dM}{d\phi} \right) . \qquad (136)$$

Nadai also derives the following relation:

$$\sigma_c = \sigma_t \frac{d\epsilon_t}{d\epsilon_c} , \qquad (137)$$

where ϵ_t, ϵ_c = unit strains in outer tension and compression fibers, respectively.

Using this expression for σ_c, Equation (135) becomes:

$$\sigma_t = \frac{1}{bh^2} \left(2M + \frac{\phi dM}{d\phi} \right) \left(\frac{1 + \dfrac{d\epsilon_t}{d\epsilon_c}}{\dfrac{d\epsilon_t}{d\epsilon_c}} \right) . \qquad (138)$$

Nadai's analysis shows that ϕ can be expressed as:

$$\phi = \frac{(\epsilon_t + \epsilon_c) \, 1}{2h} , \qquad (139)$$

where 1 = length of gage section.

In determining tensile stresses, two plots were made from the bend-test data: M versus ϕ and ϵ_t versus ϵ_c. Values of $dM/d\phi$ and $d\epsilon_t/d\epsilon_c$ were taken from tangents to these plots, and substituted into Equation (138). The resulting stresses at fracture, compared with those from the usual elastic expression, were as follows:

Specimen	Fracture Strength, psi	
Number	Equation (138)	Elastic Equation
K-OB-1	101,200	101,200
-3	100,000	100,200
-4	98,800	99,800
-5	103,700	104,200
-7	108,400	108,800
Average	102,400	102,800

These values indicate that the deviation from Hooke's Law was so slight that the errors introduced from neglecting it were negligible. The slight inaccuracies in measurements and nonuniformity between specimens undoubtedly introduce larger errors.

Friction in Bend Tests

In all bend tests to date, specimens were loaded and supported on external surfaces. There is very likely either motion or a tendency for motion in these surfaces. Such motion would be opposed by friction forces at each loading and supporting point. Effort was directed toward determining the error introduced by neglecting the effect of these forces on the stress in the extreme top or bottom fibers.

Frocht[24] briefly discusses this matter, indicating that the friction forces are as represented in Figure 6, with the force F_2 greater than F_1. The friction effect thus becomes equivalent to an axial tension force and a couple of opposite sign to that of the applied bending moment. It is particularly significant to size-effect studies that Frocht points out that the friction couple is especially pronounced in deep beams and at high loads.

If μ is the coefficient of friction at all contacts, the friction forces in Figure 6 are:

$$F_1 \leq \mu P \text{ and } F_2 \leq \mu P. \tag{140}$$

The inequalities in these expressions represent the conditions in which the tendency to move is not great enough to produce movement.

The stresses in the gage section resulting from the forces acting in Figure 9 can be determined by considering a cross section m-n. Summing moments at the neutral axis of the cross section gives $M = Pa - \left(F_2 \frac{h}{2} + F_1 \frac{h}{2}\right)$, where M is the internal moment at the cross section. The stress in the extreme top or bottom fibers of the cross section m-n then becomes:

$$\sigma = \frac{F_2 - F_1}{bd} \pm \frac{6}{bd^2} \left[Pa - \left(F_2 \frac{h}{2} + F_1 \frac{h}{2}\right) \right] . \tag{141}$$
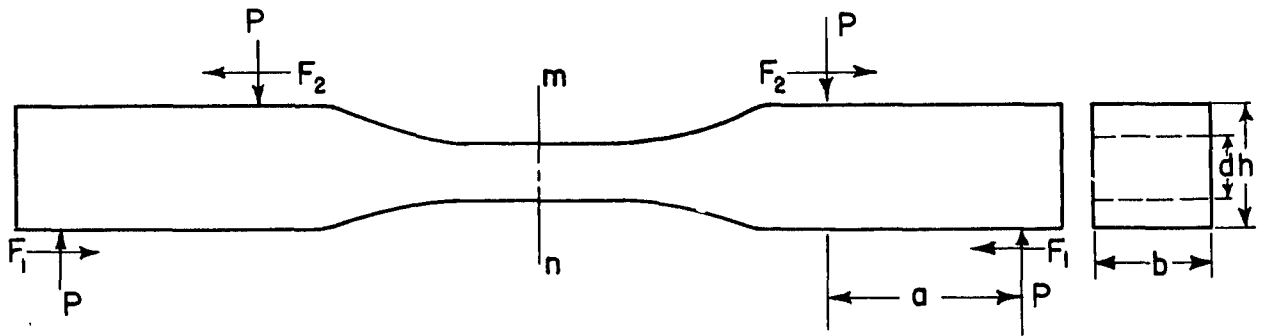
FIGURE 9. FRICTION FORCES IN THE BEND TEST

A-2193

Examination of this expression shows that, if $F_2 \neq F_1$, the stress in the top fibers will not be equal in magnitude and opposite in sign to the stress in the bottom fibers. This factor could account for the differences found in tension and compression moduli from bend tests, rather than any true difference in these moduli. The inequality $F_2 \neq F_1$ would result from unequal forces tending to produce movement, with movement suppressed at any or all contacts, or from different frictional coefficients at the contacts, with movement occurring at all contacts.

Consider the case of maximum friction in the system with the same coefficient at all contacts, i.e., $F_1 = F_2 = \mu P$. Equations (140) and (141) combine to yield:

$$\sigma = \pm \frac{6P}{bd^2} (a - \mu h) \quad . \tag{142}$$

To determine the error, this equation considering friction must be compared with the equation for stress neglecting friction. With equal moduli in tension and in compression, the latter equation is:

$$\sigma_b = \pm \frac{6Pa}{bd^2} \quad . \tag{143}$$

The error then becomes:

$$E = - \frac{\sigma - \sigma_b}{\sigma} = - \frac{\mu}{a/h - \mu} \quad . \tag{144}$$

In the bend tests on K151A reported in AF Technical Report No. 6512, a = 1 and h = 0.625. Letting μ = 0.4, the value given in Marks' Handbook for garnet on hard steel, from Equation (144), the error becomes:

$$E = - \frac{0.4}{1/0.625 - 0.4} = - 0.333 \text{ or} = - 33.3\% \quad .$$

This means that superposed stresses could have opposed the bending stresses in the extreme fibers in an amount to make the actual stresses as little as three-fourths of those recorded. The fact that the compression and tension moduli in bend tests to date have always been unequal, and that they agree fairly well with those obtained from direct tension or compression tests, establishes that the error was much less than this calculated, 33.3%. However, the possible friction effect certainly becomes of great concern in this work where precise data are required, particularly in view of the great error it apparently is capable of introducing.

Experiments also were made in the interests of establishing the effect of friction on recorded bend-test data. Stress-strain curves were obtained from bend tests on three K151A specimens in the same manner as used to obtain the values in Table 5. Each specimen was loaded three times to a maximum stress of about 55,000 psi. A stress-strain curve was plotted for each loading. This procedure was duplicated on each specimen with all contact surfaces greased with High-Pressure Lubriko M-6, a product of Master Lubricant Company. All surfaces of the loading yoke and supporting jig where lateral movement or rolling might occur were greased.

No significant differences could be detected between comparable stress-strain curves with greased or ungreased contacts. Both tension and compression curves were obtained. Values of Young's modulus from the data are given in Table 8.

These data indicate either that no movement occurred or that friction effects are not significant. If there had been any movement, the grease would be expected to reduce the friction forces, causing a change in the value of Young's modulus if these forces were appreciable. On the other hand, the forces tending to produce movement may have been insufficient to overcome friction even with the surfaces greased. In this case, the error would not be changed by the greasing.

On this basis, the maximum possible error from friction as given by Equation (144) does not appear to be present.

TABLE 8.   YOUNG'S MODULUS OF K151A FROM BEND
TESTS WITH GREASED AND UNGREASED
CONTACT SURFACES

| Specimen No. | Young's Modulus, 10^6 psi | | | |
| | Greased Surfaces | | Ungreased Surfaces | |
	Tension	Compression	Tension	Compression
12	57.0	57.0	57.0	57.0
13	55.0	56.0	57.0	56.8
14	55.7	55.7	55.7	55.7

Effect of Strain Rate

Before the resistance of ceramics to load can be defined, the effect of strain rate, among other factors, must be established. Detailed research on strain rate is contemplated as the next new phase of this project. A preliminary experiment was made during the period of this report.

In this experiment, two groups of Hydrostone specimens were fractured in the tension test with the crosshead speed as the only known variable between the two groups. In one case, the speed was 0.005 inch per minute and, for the other group, it was 1.00 inch per minute. The loading, of course, was continuous, rather than incremental.

Table 9 gives the results. It is surprising that the specimens tested with the greater strain rate had the lower strengths. This behavior is contrary to the results of other experimenters[25]. No suitable explanation is apparent at this time. As indicated previously, however, the future program for this project contemplates a much more thorough examination of strain-rate effects.

Bend Tests on Porcelain

A new material was introduced into the program during the year with initial tests of a high-alumina spark-plug porcelain, produced by Champion Spark Plug Company. As pointed out earlier, probably as high a degree of control is used in the manufacture of this material as any ceramic product.

TABLE 9. EFFECT OF STRAIN RATE ON THE STRENGTH OF HYDROSTONE IN TENSION

Specimen Number	Crosshead Speed, in. per minute	Strength, psi
SEL-1-29	0.005	1142
SEL-1-38	0.005	1099
SEL-1-25	0.005	1105
SEL-1-36	0.005	1184
SEL-1-42	0.005	1119
SEL-1-21	0.005	1073
SEL-1-28	0.005	1073
	Average	1113.6
	Standard Deviation =	35.3
SEL-1-34	1.00	725
SEL-1-26	1.00	776
SEL-1-33	1.00	934
SEL---42	1.00	864
SEL-1-20	1.00	803
SEL---43	1.00	874
SEL-1-27	1.00	858
	Average	833.4
	Standard Deviation =	65.04

For this reason, it is particularly attractive in the interests of reducing the effect of material variables from the data obtained for this project. Also, it represents a larger class of ceramic bodies than either the K151A or plaster, the only materials used for the past two years.

Initial tests indicated good reproducibility and the ability to fabricate specimens of the required complex shapes to the desired tolerances. Specifically, 23 specimens gave an average strength of 33,520 psi with a standard deviation of 2,205 psi when fractured in the bend test. Six determinations of Young's modulus in the bend test gave values ranging from 40.0×10^6 to 43.8×10^6 psi in tension and from 40.6×10^6 to 43.6×10^6 psi in compression. Stress was proportional to strain up to fracture in each case.

DEVELOPMENT AND REFINEMENT OF TESTS

The precise measurement of stress and strain under various controlled conditions is required to meet the objectives of this project. Problems in testing methods are introduced by this requirement. Effort during the past year to solve these problems is covered in this section.

Torsion Test

The twisometer described in AF Technical Report No. 6512, used for measuring twist in the torsion test, was modified during the year. Owing to repeated failures and irregular behavior, the electronic system for measuring the optical levers was abandoned. For the replacement, the light beams from each of the two mirrors mounted on the specimen were intercepted by a flat screen, and the vertical distance between the two resulting light spots measured.

Also, the torquemeter used in the torsion test was found to be slightly, but objectionably, unstable. To correct this condition, the cantilever beam with attached strain gages was replaced with a mirror mounted on the dynamometer bar. The image of an illuminated scale was viewed in the mirror with a telescope. Twisting of the bar produced by the torque was indicated on the scale, such that calibrations showed 0.01 inch of the scale to be equivalent to eight inch-pounds of torque. Scale divisions of 0.05 inch could be read with the telescope to ±0.01 inch.

Tension Test

The modified Martens extensometer for high-temperature tension tests described in AF Technical Report No. 6512 was calibrated. The equipment functioned satisfactorily in a trial run at 800 F.

Figure 10 shows the arrangement of this strain-measuring system. The telescope and scale are mounted rigidly on the wall to insure that the lengths of the various optical levers do not change, thus maintaining a constant calibration factor for a given set of mirrors.

The system was calibrated with SR-4 strain gages, using a steel specimen at room temperature. A linear relationship existed between the two strain-measuring devices. A one-inch change in scale reading being equivalent to 75 microinches per inch of strain, as measured by the SR-4 gages. The scale readings could be estimated to 1/8 inch of change, equivalent to about 9 microinches per inch.

Vibration from the hydraulic pump of the testing machine had to be damped out for satisfactory performance of the extensometer. Brass fins on each extensometer arm, extending down into a cup of oil, accomplished the damping without interfering with the normal movement of the arms.

From the trial runs, the extensometer appears to have the following advantages:

1. Ability to measure small extensions

2. Usefulness at high temperatures, probably up to 2200 F with sapphire rods and refractory clamps

3. No complex electrical circuits

4. Ease of extending its range with little loss of sensitivity, by using larger mirror shafts

On the other hand, poor features of the extensometer are as follows:

1. Extreme care is required in setting up

2. Two operators are required for continuous-loading tests

3. High-quality mirrors are required and the diameter of the mirror shafts is very critical. Each mirror-shaft combination must be calibrated separately

The sensitivity, which is independent of temperature, is felt to outweigh the disadvantages and to warrant use of the extensometer.
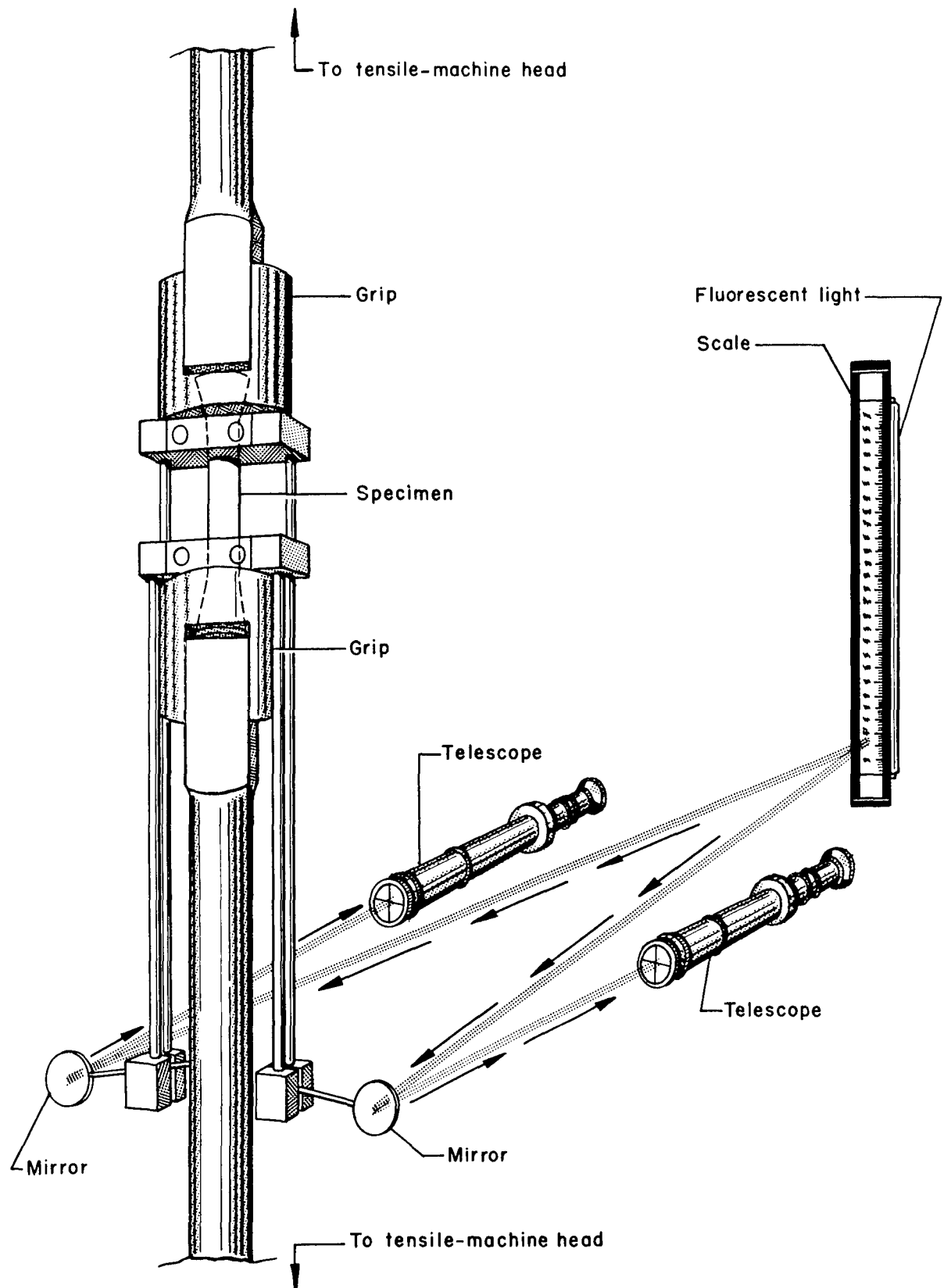
To tensile-machine head

Grip

Fluorescent light

Scale

Specimen

Grip

Telescope

Telescope

Mirror

Mirror

To tensile-machine head

FIGURE IO. HIGH-TEMPERATURE EXTENSOMETER

B-2194

Attempted size-effect experiments on plaster using the tension test failed to produce acceptable data. Difficulties with stress concentrations at the grips and with superposed bending were encountered. One of these difficulties resulted from surface discontinuities at the parting lines of the molds. To reduce these defects, the specimen design was changed from circular to rectangular cross sections. With the new design, all parting lines in the molds could be placed at corners. No tests have been made using the new design.

A photoelastic study was made of bending in the tension test. The model was cut from a sheet of CR-39 resin so as to have a rectangular gage section of 3/8 x 1/2 inch. Otherwise, the model was the same as the tension specimen described in AF Technical Report No. 6512.

Small holes, 0.019 inch in diameter, were drilled in the gage section of the model. These holes were to act as stress concentrators and, thereby, produce a fringe pattern which would become asymmetrical if an eccentric load were applied. Although this scheme produced the desired results, a more sensitive indicator of eccentric loading was found. When a specimen of any photoelastic material is being subjected to uniform tension, a uniform shading exists at all times. But, with an eccentric load, dark and light areas coexist in the specimen.

The results indicated that, with normal precautions in placing the tension specimen in the grips, the stress is distributed uniformly automatically, and this uniform distribution is retained as the load is increased. However, if the grips are not aligned, the stress is nonuniform, and remains nonuniform with any shifting of the adaptor rods in the ball-and-socket joints.

Bend Test

Photoelastic studies also were made on bend-test models. The models were cut from a sheet of CR-39 resin, 3/8 inch thick. Three models were the same except for depth. The depths of the gage sections of these specimens were 1/4 inch, 1/2 inch, and 3/4 inch. The gage sections were connected to the shoulder sections by elliptical fillets. The span between loading points was 3 inches and that between the supporting points was 5 inches.

Each model was loaded so as to produce a stress of 2700 psi in the outer fibers of the gage section. The resulting fringe patterns are shown in Figures 11, 12, and 13. It was noted in these tests that:

   1.   The fringe patterns came in evenly upon application of load;
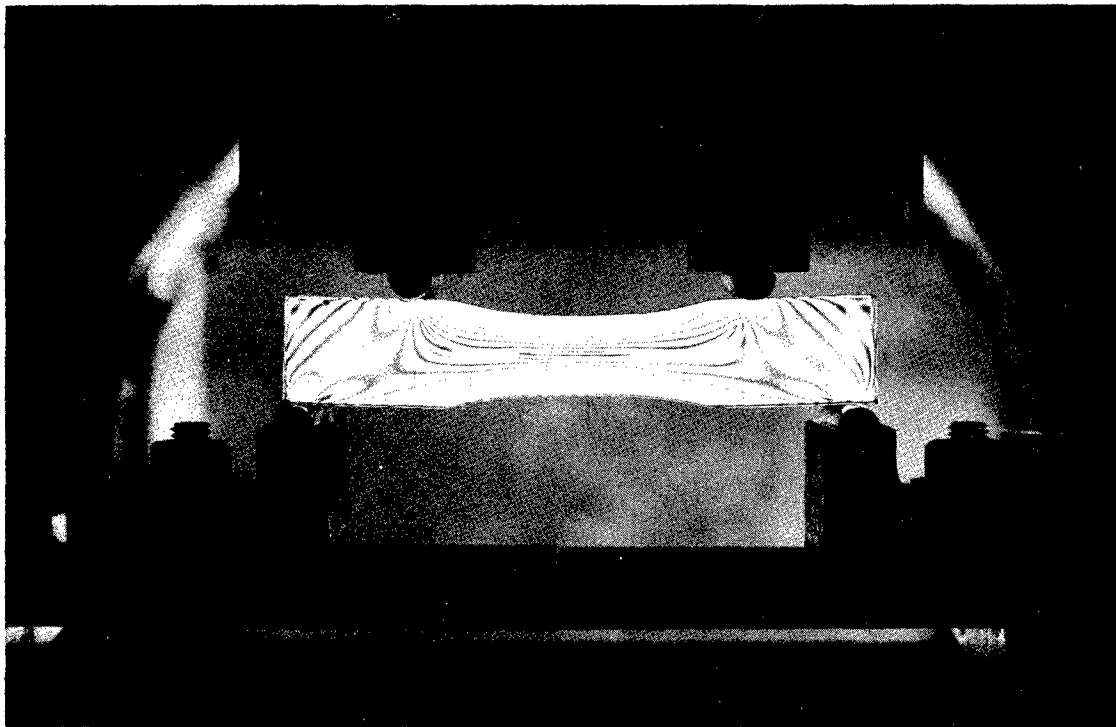   hence, the stress was proportional to the load
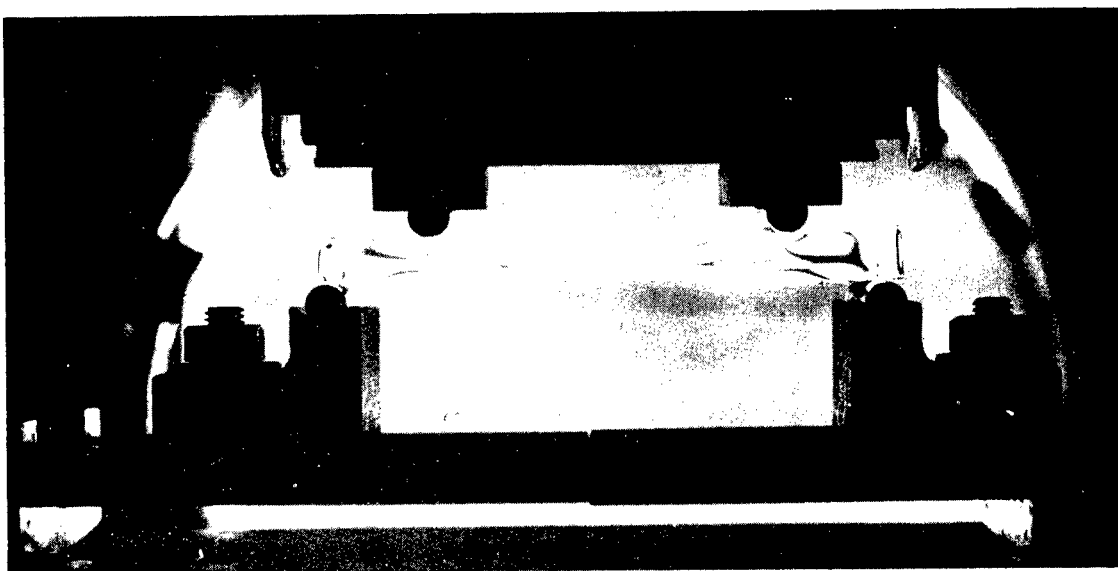
79556

FIGURE 11. STRESS PATTERN IN BEND-TEST
MODEL HAVING 1/4-INCH DEPTH
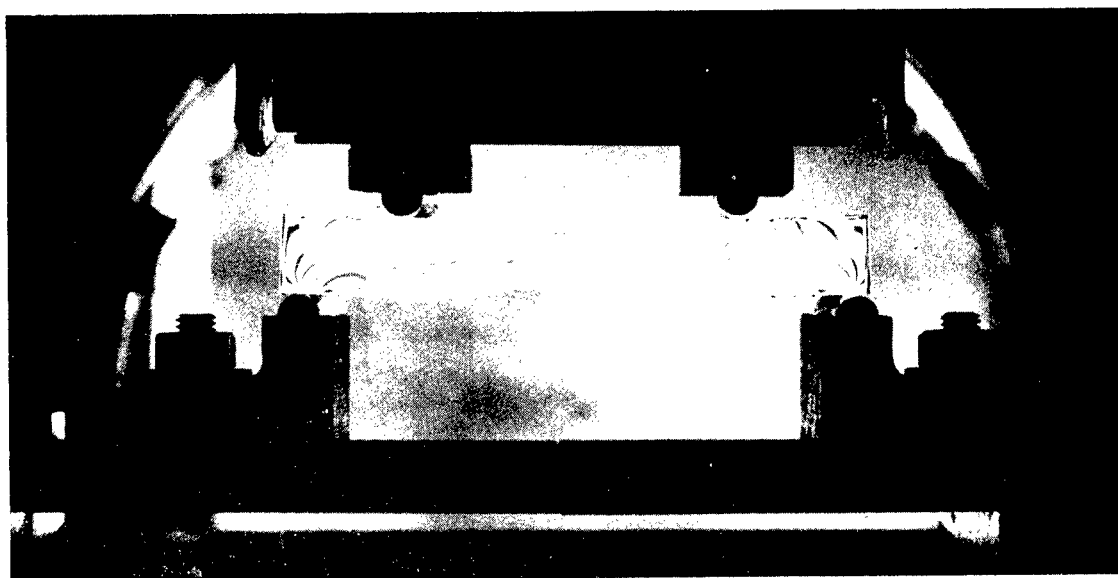
79558

FIGURE 12. STRESS PATTERN IN BEND-TEST
MODEL HAVING 1/2-INCH DEPTH

79559

FIGURE 13.   STRESS PATTERN IN BEND-TEST
   MODEL HAVING 3/4-INCH DEPTH

2.   There were no stress concentrations in the gage sections

3.   Within the limits of the technique, the stresses in the top
     and bottom outermost fibers were equal.

Consideration also was given to the effect of the inner fibers on bend-
test data. For a bend test, the stress distribution is such that the high
stresses occur in the outer fibers. It follows that fracture logically should
start at or near the surface; however, the inner fibers, which are at lower
stresses, may exert an influence on the strength of the beam. Ideally, an
I-beam with a web of zero thickness would eliminate the influence of inner
fibers. A bend test on such a specimen would approach a compression test
in one flange, and in the other flange, a tension test. A tentative design
was developed with a modification of such an I-beam as the gage section.
Fabrication problems have delayed the construction of such a specimen.

A new bending jig was designed and built. This new jig, which is
shown in Figure 14, is similar to the bend jig described in AF Technical
Report No. 6512, in operating principle, except that its construction per-
mits the loading points and supporting points to translate with more freedom
as the specimen deflects. Each of these points is supported on ball bearings.
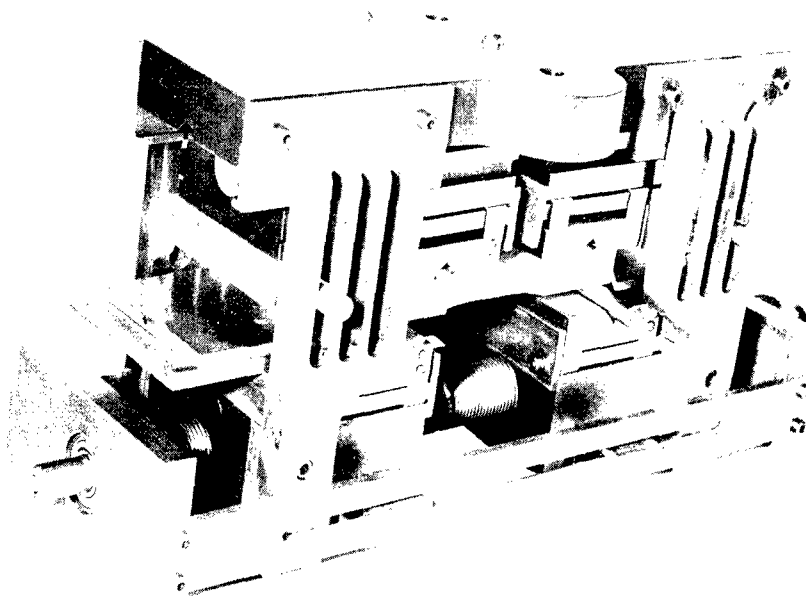
89148
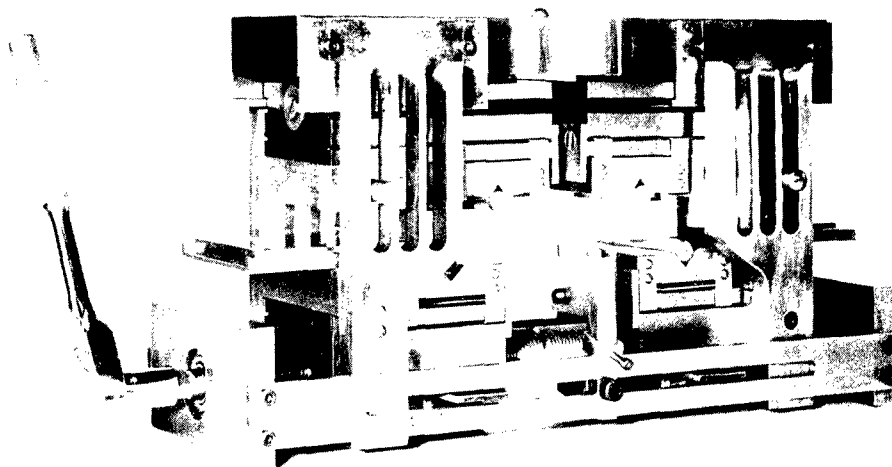
89150

FIGURE 14. JIG FOR LOADING BEND-TEST SPECIMENS

Special provisions also were made for ease in setting up for testing. Since the jig permits the loading and supporting points to move axially on ball bearings, it tends to alleviate the frictional forces present.

Combined-Stress Testing

A determination of the validity of the various fracture theories involves a series of tests in which the state of stress existing at the point at which fracture initiates is known. The most general state of stress is that of triaxial stress in which, at the point considered, there are stresses acting on any three mutually perpendicular planes. Obviously, the most desirable type of test would be one in which a triaxial state of stress exists. Several difficulties confront triaxial testing, however. To indicate the areas in which the difficulties are likely to arise, the following points are included:

1. The design of a specimen in which the true state of stress causing fracture is known. Most proposed designs introduce extraneous stresses which are difficult to determine.

2. In a specimen in which a uniform state of stress does not exist from point to point, fracture is initiated at a critical local region. The effect on the ultimate failure of the specimen of the surrounding regions which are not in a critical state is vague.

3. Strain measurements at what would be considered the gage region would be difficult.

4. In the theory of fracture, a so-called surface of rupture exists. Mathematically, this is expressed as $F\left(\sigma_1, \sigma_2, \sigma_3\right) = 0$, where $\sigma_1, \sigma_2, \sigma_3$ are principal stresses. In testing, a limitation arises from the fact that a given type of test will explore only a part of the total surface.

5. The path of loading should be a straight line from the origin to the point of fracture in the $\sigma_1, \sigma_2, \sigma_3$ - axis system. This requires that loading devices must be coordinated so as to apply the load in a predetermined manner.

It is of interest to note that little triaxial testing has been conducted which has been considered both complete and satisfactory. In each case, either the results are thought to be of questionable validity or they cannot be interpreted. A detailed discussion of these tests is given by Nadai[4].

As a consequence of the difficulties involved in triaxial testing, it is felt that, for the present, combined-stress tests should be limited to biaxial testing, for which some of the above difficulties are not present. Specifically, Items 1, 2, and 3 can be eliminated partially or wholly.

Capacitance Micrometer

Preliminary trials of the capacitance micrometer described in AF Technical Report No. 6512 were made at 300 F. In these trials, the micrometer was stable; switching the furnace power on and off had little effect on its behavior.

In this micrometer, strain or contraction of the specimen causes a decrease in the spacing between two parallel capacitor plates, resulting in a change of capacitance. This change is translated into a voltage difference, which is measured by a suitable recorder. The calibration setup utilizes a fine-thread screw feed to regulate the spacing between the capacitor plates. The movement of the screw feed, and hence, the change of capacitor-plate spacing, is measured by a dial gage outside the furnace. With this calibration setup, the relationship of change in capacitor-plate spacing, or strain, and response of the capacitance micrometer was determined directly.

BIBLIOGRAPHY

1.   Bridgman, P. W., "The Effect of Hydrostatic Pressure on the Fracture of Brittle Substances", J. Appl. Physics, 18, 2, p 246, 1947.

2.   Timoshenko, S., Strength of Materials, Part II, 2nd Ed., p 481, D. Van Nostrand Company, New York, 1941.

3.   Marin, J., "Working Stresses for the Rational Design of Concrete Structures", J. Appl. Physics, 9, 1, p 49, 1938.

4.   Nadai, A., Theory of Flow and Fracture of Solids, 1, 2nd Ed., p 103, McGraw-Hill Book Company, New York, 1950.

5.   Inglis, C. E., "Stresses in a Plate Due to the Presence of Cracks and Sharp Corners", Trans. Inst. Naval Architects, 55, Part I, p 219, 1913.

6.   Holland, A. J., and Turner, W. E. S., "The Effect of Width on the Breaking Strength of Sheet Glass", J. Soc. Glass Tech., 20, p 72, 1936; "The Breaking Strength of Glass – The Effect of Flaws and Scratches", J. Soc. Glass Tech., 20, p 279, 1936.

7.   Griffith, A. A., "The Phenomena of Rupture and Flow in Solids", Phil. Trans. Royal Soc., 221A, p 163, 1920; "Theory of Rupture", Proc. First Inter. Congress Appl. Mech., p 55, 1924.

8.   Smekal, A., "The Influence of Specimen Width on the Breaking Strength of Sheet Glass", J. Soc. Glass Tech., 20, p 449, 1936.

9.   Smekal, A., "The Nature of the Mechanical Strength of Glass", J. Soc. Glass Tech., 20, p 432, 1936.

10.   Poncelet, E. F., "Fracture and Comminution of Brittle Solids", Metals Tech., 11, No. 3, T. P. 1684, 1944.

11.   Weibull, W., "A Statistical Theory of the Strength of Materials", Ingen – Vetensk – Alcad., No. 151, 1939.

12.   Tucker, J., Jr., "The Compressive Strength Dispersion of Materials With Applications", J. Franklin Inst., 204, p 751, 1927; "Effect of Dimensions of Specimens Upon the Precision of Strength Data", Proc. ASTM, 45, p 952, 1945; "The Maximum Stresses Present at Failure of Brittle Materials", Proc. ASTM, 45, p 961, 1945.

13.   Tippett, L. H. C., "On the Extreme Individuals and the Range of Samples Taken From a Normal Population", Biometrika, 17, p 364, 1925.

14.   Frankel, J. P., "Relative Strengths of Portland Cement Mortar in Bending Under Various Loading Conditions", J. Am. Concrete Inst., 45, p 21, 1948.

15.   Arrhenius, S. Z., Physik Chem., 4, p 226, 1889.

16.   Glasstone, S., Laidler, K. J., and Eyring, H., The Theory of Rate Processes, McGraw-Hill Publ. Co., New York, 1941.

17.   Machlin, E. S., and Norwick, A. S., "Stress Rupture of Heat-Resisting Alloys as a Rate Process", Metal Technology, T. P. 2137, February, 1947.

18.   Gibbs, P., and Cutler, I. B., "On the Fracture of Glass, Which is Subjected to Slowly Increasing Stress", Technical Report No. 13, University of Idaho, August 13, 1950.

19.   Cox, S. M., "A Kinetic Approach to the Theory of Strength of Glass",
      J. Soc. Glass Tech., 32, p 127, 1948.

20.   Poncelet, E. F., "A Theory of Static Fatigue for Brittle Solids",
      Fracturing of Metals, ASM, p 201, 1948.

21.   Saibel, E., "The Speed of Propagation of Fracture Cracks",
      Fracturing of Metals, ASM, p 225, 1948.

22.   Duckworth, W. H., "Precise Tensile Properties of Ceramic Bodies",
      J. Am. Ceram. Soc., 34, p 1, 1951.

23.   Nadai, A., Ibid., p 356.

24.   Frocht, M. M., Photoelasticity, 1, pp 380-381, Wiley & Sons, Inc.,
      London, 1941.

25.   Nadai, A., Ibid., pp 187-188.